nature communications

Article

https://doi.org/10.1038/s41467-024-51860-2

# SLC13A3 is a major effector downstream of activated β-catenin in liver cancer pathogenesis

Received: 17 June 2023

Accepted: 20 August 2024

Published online: 30 August 2024

Check for updates

Wennan Zhao[1], Xue Wang[2,3], Lifeng Han[4], Chunze Zhang[5], Chenxi Wang[4], Dexin Kong[6], Mingzhe Zhang[1], Tong Xu[1], Gen Li[1], Ge Hu[1], Jiahua Luo[1], Sook Wah Yee[7], Jia Yang[7], Andreas Stahl[2], Xin Chen[3,7] ✉ & Youcai Zhang[1] ✉

Activated Wnt/β-catenin pathway is a key genetic event in liver cancer development. Solute carrier (SLC) transporters are promising drug targets. Here, we identify SLC13A3 as a drug-targetable effector downstream of β-catenin in liver cancer. *SLC13A3* expression is elevated in human liver cancer samples with gain of function (GOF) mutant *CTNNB1*, the gene encoding β-catenin. Activation of β-catenin up-regulates *SLC13A3*, leading to intracellular accumulation of endogenous SLC13A3 substrates. SLC13A3 is identified as a low-affinity transporter for glutathione (GSH). Silencing of *SLC13A3* downregulates the leucine transporter *SLC7A5* via c-MYC signaling, leading to leucine depletion and mTOR inactivation. Furthermore, silencing of *SLC13A3* depletes GSH and induces autophagic ferroptosis in β-catenin-activated liver cancer cells. Importantly, both genetic inhibition of *SLC13A3* and a small molecule SLC13A3 inhibitor suppress β-catenin-driven hepatocarcinogenesis in mice. Altogether, our study suggests that SLC13A3 could be a promising therapeutic target for treating human liver cancers with GOF *CTNNB1* mutations.

Liver cancer is the third leading cause of cancer-related deaths worldwide, with hepatocellular carcinoma (HCC) accounting for 75-85% of all liver cancer cases[1]. Gain-of-function (GOF) mutations in *CTNNB1*, the gene encoding β-catenin, have been detected in over 80% of pediatric liver cancers and 20–40% of adult liver cancers[2]. Given the crucial role of hyperactivated Wnt/β-catenin signaling in the stemness, progression, metastasis, and drug resistance of liver cancer, various Wnt/β-catenin inhibitors have been investigated for their potential in liver cancer treatment[3,4]. However, none of these inhibitors have achieved clinical approval because they typically target the β-catenin complex or the pathways upstream of β-catenin, which unavoidably results in on-target toxicities in normal cells[2]. Therefore, studies focusing on the identification of drug-targetable effectors downstream of β-catenin are urgently needed.

Solute carrier (SLC) transporters regulate the import and efflux of diverse solutes, metabolites, ions, and drugs across the cell membrane. SLC transporters serve as significant targets for drug development[5]. Remarkable alterations in the expression patterns of SLC transporters have been reported in various cancers, including liver cancer[6]. Solute carrier family 13 member 3 (SLC13A3), also known as sodium-dependent dicarboxylate transporter (NaDC3), is highly expressed in the liver[7]. Bidkhori et al. identified three HCC subtypes (iHCC1-3)

[1]School of Pharmaceutical Science and Technology, Tianjin University, Tianjin, China. [2]Department of Nutritional Sciences and Toxicology, University of California Berkeley, Berkeley, CA, USA. [3]Cancer Biology Program, University of Hawaii Cancer Center, Honolulu, HI, USA. [4]Tianjin State Key Laboratory of Modern Chinese Medicine, Tianjin University of Traditional Chinese Medicine, Tianjin, China. [5]Department of Colorectal Surgery, Tianjin Union Medical Center, Tianjin, China. [6]Tianjin Key Laboratory on Technologies Enabling Development of Clinical Therapeutics and Diagnostics, School of Pharmacy, Tianjin Medical University, Tianjin, China. [7]Department of Bioengineering and Therapeutic Sciences, University of California, San Francisco, CA, USA.
✉e-mail: xinchen3@hawaii.edu; youcai.zhang@tju.edu.cn

through a comprehensive analysis of The Cancer Genome Atlas-Liver Hepatocellular Carcinoma (TCGA-LIHC) dataset, and demonstrated that *SLC13A3* mRNA expression is substantially high in the iHCC2 subtype with a high incidence of *CTNNB1* mutations[8]. Additionally, Charawi et al. reported that *SLC13A3* is highly expressed in *CTNNB1*-mutated HCCs[9]. However, the association of SLC13A3 with β-catenin and the functional role of SLC13A3 in HCCs need further elucidation.

In this work, we show that SLC13A3 is a drug-targetable effector downstream of β-catenin. Our findings reveal that *SLC13A3* expression is upregulated in β-catenin-activated human HCCs. SLC13A3 plays a pivotal role in regulating intracellular leucine, which promotes β-catenin-driven hepatocarcinogenesis in mice. Additionally, we demonstrate that SLC13A3 functions as a low-affinity transporter for glutathione (GSH). Inhibiting SLC13A3 induces autophagic ferroptosis in β-catenin-activated liver cancer cells and significantly impedes β-catenin-driven hepatocarcinogenesis in preclinical models.

## Results

### *SLC13A3* expression correlates with *CTNNB1* GOF mutations in human HCC specimens

To investigate the clinical significance of SLC13A3 in human HCC, we analyzed *SLC13A3* mRNA expression in patient samples using HCCDB, a database archived 15 public HCC gene expression datasets (http://lifeome.net/database/hccdb/home.html). Analysis of the HCCDB3 dataset revealed that *SLC13A3* mRNA expression was upregulated in cirrhotic tissues ($n = 40$) and further increased in HCC tissues ($n = 268$) compared to healthy tissues ($n = 6$) (Supplementary Fig. 1a). *SLC13A3* mRNA expression was significantly upregulated in HCC tissues ($n = 268$) compared to paratumor adjacent tissues ($n = 243$). Analysis of the other six HCCDB datasets, containing a total of 1046 HCC tissues and 588 paratumor adjacent tissues, also showed a significant upregulation of *SLC13A3* mRNA expression in HCC tissues (Supplementary Fig. 1b). Co-expression network analysis of all HCCDB datasets revealed a substantial interaction between *SLC13A3* and several canonical β-catenin target genes, such as *LGR5*, *TBX3*, and *GLUL* (Supplementary Fig. 1c).

We further conducted a comprehensive analysis of *SLC13A3* mRNA expression using TCGA-LIHC dataset. Among the top 20 genes, *SLC13A3* was the only SLC gene whose mRNA expression exhibited a positive correlation with all three β-catenin target genes (*LGR5*, *TBX3*, and *GLUL*) (Supplementary Data 1). Analysis through cBioPortal revealed that the frequency of *SLC13A3* genetic alteration (5.3%) was comparable to that of *TBX3* (6%) and *LGR5* (6%) (Supplementary Fig. 2a). Correlation analysis of *SLC13A3* expression with HCC common genetic events revealed that HCCs with high *SLC13A3* expression were mainly characterized by *CTNNB1* mutations (Fig. 1a). Compared to normal adjacent tissues ($n = 50$), *SLC13A3* mRNA expression was higher in *CTNNB1* mutant HCCs ($n = 96$), but lower in non-*CTNNB1* mutant HCCs ($n = 275$) (Fig. 1b). Similar results were observed when comparing HCC tissues with their paired nontumorous tissues (Fig. 1c). In TCGA-LIHC dataset, *SLC13A3* mRNA expression correlated positively with 1324 genes ($r \geq 0.2$) and negatively with 2087 genes ($r \leq -0.2$) (Supplementary Data 2 and 3). As anticipated, the canonical Wnt/β-catenin targets were among the top 20 *SLC13A3* positively correlated genes, such as *LGR5*, *CYP2E1*, *RHBG*, *TBX3*, *AXIN2*, *GLUL*, and *SP5* (Supplementary Fig. 2b). KEGG pathway analysis showed that genes positively correlated with *SLC13A3* were significantly enriched in various metabolic pathways, whereas genes negatively correlated with *SLC13A3* were most significantly enriched in the "cell cycle" (Fig. 1d). This suggests a potential role of SLC13A3 in HCC metabolism and growth.

We next examined SLC13A3 protein levels in 82 paired human HCC and matched normal adjacent liver tissues using immunohistochemistry (IHC). Among the 82 HCC tissues examined, nuclear β-catenin expression was observed in 11 cases, cytoplasmic β-catenin expression in 12 cases, and membranous β-catenin expression in 59 cases (Supplementary Fig. 2c). Notably, SLC13A3 protein levels were higher in HCCs with cytoplasmic/nuclear β-catenin expression compared to their paired normal counterparts (Fig. 1e and Supplementary Fig. 2c). The cytoplasmic/nuclear expression of β-catenin corresponds to the hyperactivation of Wnt/β-catenin signaling. We found that cytoplasmic/nuclear accumulation of β-catenin was significantly associated with SLC13A3 overexpression ($R = 0.9084$, $P < 0.0001$) (Fig. 1f). Log-rank (Mantel–Cox) test analysis revealed that HCC patients with high SLC13A3 protein levels had significantly reduced overall survival compared to those with low SLC13A3 levels (Fig. 1g). Altogether, these findings suggest that *SLC13A3* expression is upregulated in β-catenin-activated HCCs.

### *SCL13A3* is a direct downstream target of β-catenin

Based on the clinical findings, we hypothesized that *SLC13A3* expression could be up-regulated by β-catenin activation. Firstly, the protein level of SLC13A3 was examined in eight liver cancer cell lines (Supplementary Fig. 3a). SLC13A3 protein levels were high in GOF *CTNNB1* mutant cells (HepG2, Huh6, and SNU398), but low in non-*CTNNB1* mutant cells. Secondly, the effect of β-catenin activation was evaluated in non-*CTNNB1* mutant Huh7 and HLF cells by either transfection with a mutant *CTNNB1*-expressing plasmid or treatment with the β-catenin activator lithium chloride. The forced expression of mutant *CTNNB1* significantly increased the expression of *SLC13A3* and two known β-catenin target genes (*TBX3* and *GLUL*) (Fig. 2a). Treatment with lithium chloride also markedly increased the mRNA expression of *SLC13A3*, *TBX3*, and *GLUL* (Supplementary Fig. 3b). Finally, the effect of *CTNNB1* knockdown was examined in GOF *CTNNB1* mutant HepG2 and SNU398 cells. Among the three *CTNNB1*-specific short hairpin (sh) RNAs, the sh*CTNNB1*#2 had the most prominent knockdown effect and was thus used for subsequent experiments (Supplementary Fig. 3c). qRT-PCR and western blot analyses revealed that knockdown of *CTNNB1* significantly reduced *SLC13A3* expression in HepG2 and SNU398 cells (Fig. 2b).

Upon activation, β-catenin accumulates in the nucleus and binds to T-cell factor/lymphoid enhancer factor (TCF/LEF) transcription factors to recruit coactivators, leading to the transcription of β-catenin target genes. We located the 1.0 kb region upstream of the transcription start site (TSS) in *SLC13A3* promoter region using the Eukaryotic Promoter Database (http://www.epd.isb-sib.ch), and predicted the putative TCF4 binding sites using PROMO website (https://alggen.lsi.upc.es/) (Supplementary Fig. 3d). A consensus TCF-binding element (TBE, 5′-CTTTGTT-3′) was identified in the promoter region (−243 to -−237 bp upstream of the TSS). To determine whether β-catenin regulates the promoter activity of *SLC13A3*, we generated a series of luciferase reporter plasmids containing different promoter regions (Fig. 2c). The reporter activity of the wild-type (WT) *SLC13A3* promoter was significantly greater than that of the empty vector in β-catenin-activated HEK293 cells. As anticipated, deletion of the consensus TBE markedly decreased the *SLC13A3* promoter activity. We also identified a second putative β-catenin binding site (−68 to −41 bp upstream of the TSS) in the *SLC13A3* promoter region. ChIP-PCR assay analysis in HepG2 cells demonstrated the ability of β-catenin to recognize both binding sites (Fig. 2d). In contrast, ChIP-PCR assay using anti-TCF4 antibody revealed a strong band for the consensus TBE, but a much weak band for the second β-catenin binding site. As specific controls, no bands were amplified with primers spanning −2100 to −2081 bp upstream of the TSS in the *SLC13A3* promoter region or with primers for the *GAPDH* promoter region. Furthermore, in vitro EMSA assay was performed to show that only the consensus TBE binds TCF4 protein (Fig. 2e), indicating that the second β-catenin binding site was not a typical TBE. Nonetheless, these findings suggest that β-catenin /TCF4 can directly bind to the promoter of *SLC13A3*.

https://doi.org/10.1038/s41467-024-51860-2

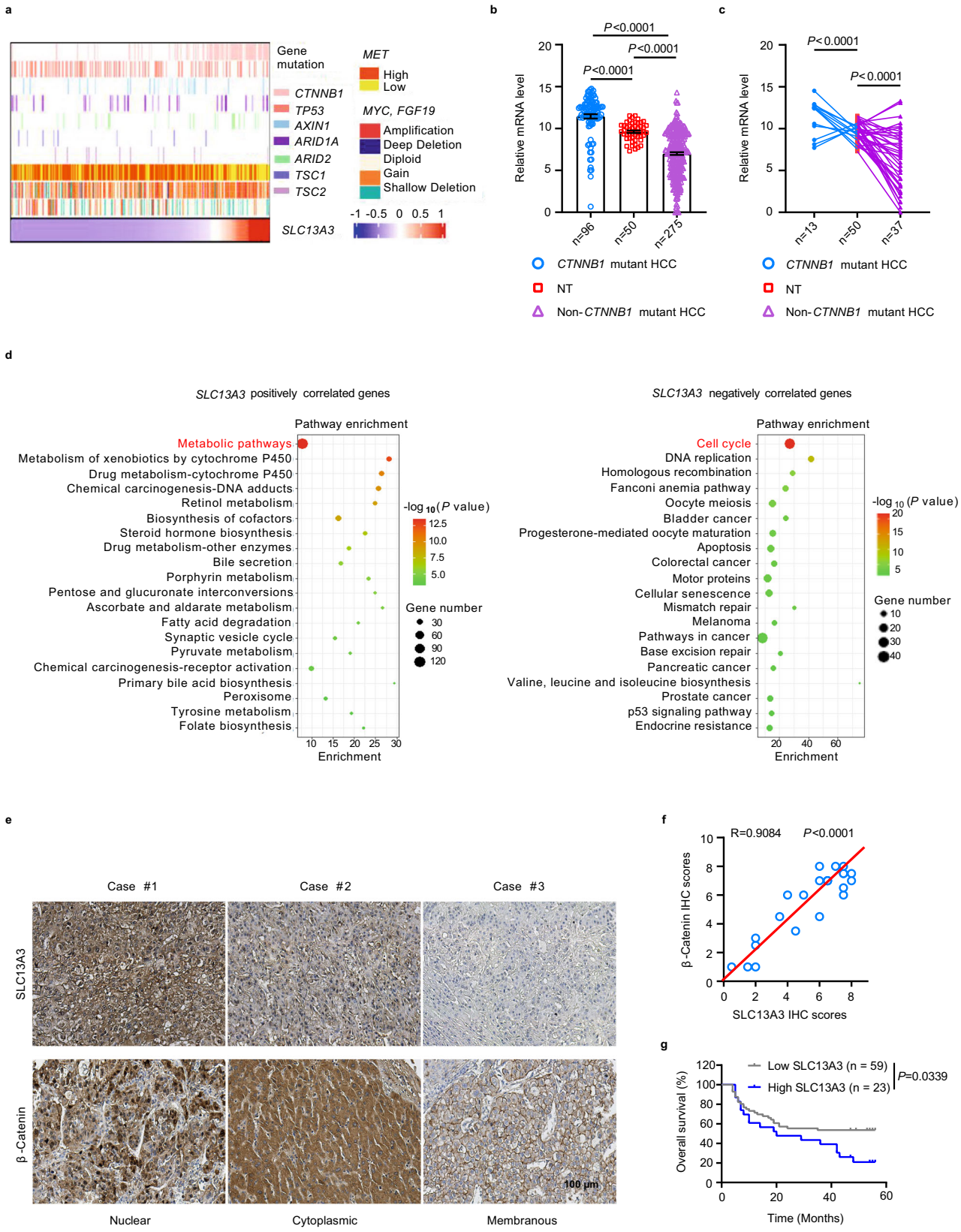


SLC13A3 is known to transport the tricarboxylic acid (TCA) cycle intermediates, particularly dicarboxylates[7]. To determine whether β-catenin regulates the SLC13A3 activity, we investigated the global metabolomic alterations after overexpression of mutant *CTNNB1* in non-*CTNNB1* mutant Huh7 cell (Huh7-*EV* vs Huh7-*CTNNB1*) and knockdown of *CTNNB1* in GOF *CTNNB1* mutant HepG2 cells (HepG2-sh*NC* vs HepG2-sh*CTNNB1*) (Supplementary Fig. 4a, b). We found that the intracellular concentrations of several SLC13A3 substrates, such as malate, succinate, and fumarate, were significantly increased with *CTNNB1* overexpression in Huh7 cells and decreased with *CTNNB1* knockdown in HepG2 cells (Fig. 2f). Collectively, these findings suggest that β-catenin regulates both SLC13A3 expression and activity in liver cancer cells.

**Fig. 1 | Clinical correlation of *SLC13A3* with *CTNNB1* in human HCC tissues.** **a** Heatmap of *SLC13A3* mRNA levels with common gene mutations based on the analysis of TCGA-LIHC dataset. The mutation data was extracted from the cBioPortal for Cancer Genomics (http://www.cbioportal.org). Heatmap was drawn using Complex heatmap analysis. **b** Relative *SLC13A3* mRNA levels in *CTNNB1* mutant HCC samples ($n = 96$ samples, blue), nontumoral tissues (NT) ($n = 50$ samples, red), and non-*CTNNB1* mutant HCC samples ($n = 275$ samples, purple) were determined by analyzing RNA-seq data from TCGA-LIHC dataset. Statistical analysis was performed using one-way ANOVA test. **c** Relative *SLC13A3* mRNA levels in nontumoral tissues (NT) ($n = 50$ samples, red) as well as their paired *CTNNB1* mutant ($n = 13$ samples, blue) and paired non-*CTNNB1* mutant ($n = 37$ samples, purple) HCC samples were determined by analyzing RNA-seq data from TCGA-LIHC dataset. Statistical analysis was performed using two-tailed Student's *t*-test. **d** Top 20 KEGG pathways enriched in *SLC13A3* positively correlated and negatively correlated genes from TCGA-LIHC dataset were visualized by scatter plots. Statistical analysis was performed using the two-sided hypergeometric test. Relative pathways enriched by KEGG analyses were shown in vertical axis. Colors represented different -$Log_{10}$ (p value), and changed from green to red indicating increasingly significant enrichment. **e** Representative IHC staining images of SLC13A3 in three HCC cases with different location of β-catenin staining (Case #1, nuclear staining; Case #2, cytoplasmic staining; Case #3: membranous staining). Scale bar, 100 μm. **f** Pearson correlation test analyzing the relationship of SLC13A3 and β-catenin immunohistochemistry (IHC) scores. SLC13A3 and β-catenin protein levels were analyzed by IHC in HCC samples including 12 cases with cytoplasmic β-catenin expression and 11 cases with nuclear β-catenin expression. IHC analyses of β-catenin and SLC13A3 proteins were scored as follows: grade 0, score = 1–2; grade 1, weak expression, score = 3–4; grade 2, moderate expression, score = 5–6; and grade 3, intense expression, score = 7–8. **g** Log-rank (Mantel–Cox) test of overall survival from HCC patients with high ($n = 23$ samples, IHC scores > 3, blue) and low ($n = 59$ samples, gray) SLC13A3 protein levels. The log-rank test was used to compare overall survival between groups. Source data are provided as a Source Data file.

## SLC13A3 regulates intracellular glutathione and leucine in β-catenin-activated liver cancer cells

Endogenous substrates of SLC transporters could be identified using transfected HEK293 cells[10]. Analysis of Human Protein Atlas (HPA) RNA-seq data indicated that *SLC13A3* was minimally expressed in normal HEK293 cells (Supplementary Fig. 5a). qRT-PCR analysis confirmed that all five *SLC13A* genes (*SLC13A1-5*) were minimally expressed in normal HEK293 cells with Ct values > 30 (Supplementary Fig. 5b). We then constructed HEK293 cells overexpressing either empty vector (HEK293-*EV*) or *SLC13A3* (HEK293-*SLC13A3*), which were validated by both qRT-PCR and western blot analyses (Supplementary Fig. 5c). Functionally, HEK293-*SLC13A3* cells had a significant increase in the uptake activity of $^{14}$C-succinate compared to HEK293-*EV* cells (Supplementary Fig. 5d). Next, the metabolomic profiles of HEK293-*EV* and HEK293-*SLC13A3* were compared using LC-MS-based metabolomics (Supplementary Fig. 5e). We identified significantly overrepresented metabolites in HEK293-*SLC13A3* cells, including N-acetylaspartate, a known substrate of SLC13A3 (Supplementary Data 4). Intriguingly, glutathione (GSH) was among the most significantly increased metabolites in HEK293-*SLC13A3* cells. GSH was reported to evoke potential-dependent inward currents in *X. laevis* oocytes overexpressing *SLC13A3*, indicating that SLC13A3 may transport GSH[11]. By utilizing transfected HEK293 cells, we demonstrated that GSH inhibited SLC13A3-mediated uptake of $^{14}$C-succinate in a dose-dependent manner, with the $IC_{50}$ of 1.89 mM (Supplementary Fig. 5f). SLC13A3-mediated uptake of isotopically labeled GSH displayed a saturation kinetics with a Km of 1.24 mM (Fig. 3a). Furthermore, GSH uptake at physiologically relevant concentrations was substantially higher in HEK293-*SLC13A3* cells compared to HEK293-*EV* cells (Fig. 3b). These findings suggest that SLC13A3 is a low-affinity GSH transporter.

To investigate the metabolic function of SLC13A3 in liver cancer, we examined the metabolomic alterations in HepG2 cells following *SLC13A3* knockdown. We obtained five *SLC13A3* shRNAs, and found sh*SLC13A3*#1 (sh#1) and sh*SLC13A3*#2 (sh#2) showed prominent knockdown effects (Supplementary Fig. 6a). We used sh#1 to establish *SLC13A3*-knockdown HepG2 cells. The metabolomic profiles of control (shNC) and *SLC13A3*-knockdown HepG2 cells were determined using LC-MS-based metabolomics (Supplementary Fig. 6b and Supplementary Data 5). Intriguingly, GSH was among the most significantly decreased metabolites induced by *SLC13A3* knockdown (Supplementary Fig. 6c). To further investigate the effect of *SLC13A3* knockdown on GSH, we utilized two *SLC13A3* shRNAs (sh#1 and sh#2) to silence *SLC13A3* in GOF *CTNNB1* mutant HepG2 and SNU398 cells (Supplementary Fig. 6d). To determine if *SLC13A3* knockdown altered exogenous GSH uptake, cells were pre-cultured in the medium with dialyzed serum, followed by incubation in the complete medium. Notably, *SLC13A3* knockdown significantly impeded the GSH accumulation in HepG2 and SNU398 cells (Supplementary Fig. 6d). To determine if *SLC13A3* knockdown altered endogenous GSH production, the expression of genes involved in GSH synthesis and recycling was measured. Intracellular GSH can be generated from both recycling of glutathione disulfide (GSSG), mediated by glutathione disulfide reductase (GSR), and de novo synthesis, catalyzed by glutamine-cysteine ligase (GCL, including a catalytic subunit GCLC and a modulatory subunit GCLM) and glutathione synthase (GSS). *SLC13A3* knockdown had no significant effect on the mRNA expression of *GSR*, *GCLC*, *GCLM*, or *GSS* in HepG2 cells, although it decreased *GCLC* and *GCLM* expression in SNU398 cells (Supplementary Fig. 6e). To determine if *SLC13A3* knockdown altered the precursors for endogenous GSH synthesis, the intracellular amino acids were analyzed using the metabolomics data from *SLC13A3*-knockdown HepG2 cells (Supplementary Fig. 6c). *SLC13A3* knockdown significantly decreased intracellular glutamate and glutamine in HepG2 cells. These findings suggest that *SLC13A3* knockdown decreases intracellular GSH likely by reducing both the activity of GSH uptake and the availability of GSH synthetic precursors.

Metabolomic data analysis showed that *SLC13A3* knockdown significantly decreased 13 amino acids, including 4 essential amino acids (EAAs), namely leucine, phenylalanine, tryptophan, and threonine (Supplementary Fig. 6c). Among them, only leucine was found to be decreased by *CTNNB1* knockdown in HepG2 cells and increased by *CTNNB1* overexpression in Huh7 cells (Supplementary Fig. 4). Therefore, we focused on the potential mechanism by which SLC13A3 regulated intracellular leucine. Mammalian cells need to take up EAAs from extracellular milieu because they are unable to produce EAAs de novo. Members of the SLC7 family (SLC7A5, SLC7A7, and SLC7A8), the SLC43 family (SLC43A1 and SLC43A2), the SLC6 family (SLC6A14 and SLC6A15), and the SLC38 family (SLC38A1–SLC38A11) have been implicated in the uptake of EAAs[12]. Among these transporters, *SLC13A3* knockdown significantly decreased the mRNA expression of *SLC7A5* and *SLC38A2* in both HepG2 and SNU398 cells (Supplementary Fig. 7a). SLC7A5 is an established leucine transporter. SLC7A5 dimerizes with SLC3A2 to function as an antiporter protein that exports glutamine to promote leucine uptake[13]. SLC38A2 and SLC1A5 can fuel SLC7A5-mediated uptake of leucine by importing glutamine[14,15]. Interestingly, *SLC13A3* knockdown also suppressed the mRNA expression of *SLC3A2* and *SLC1A5* (Supplementary Fig. 7b). Western blot analysis confirmed the decreased SLC7A5 and SLC3A2 proteins in *SLC13A3*-knockdown cells (Fig. 3c and Supplementary Fig. 7c). Consistent with *SLC7A5* downregulation, the cellular uptake of leucine was decreased in *SLC13A3*-knockdown cells (Fig. 3d). These findings suggest that SLC13A3 regulates intracellular leucine through SLC7A5.

To determine the potential mechanism for SLC13A3-mediated regulation of *SLC7A5*, we first utilized PROMO website to predict the putative transcription factors for the *SLC7A5* promoter binding. Among the 15 putative transcription factors, only *MYC* mRNA

https://doi.org/10.1038/s41467-024-51860-2

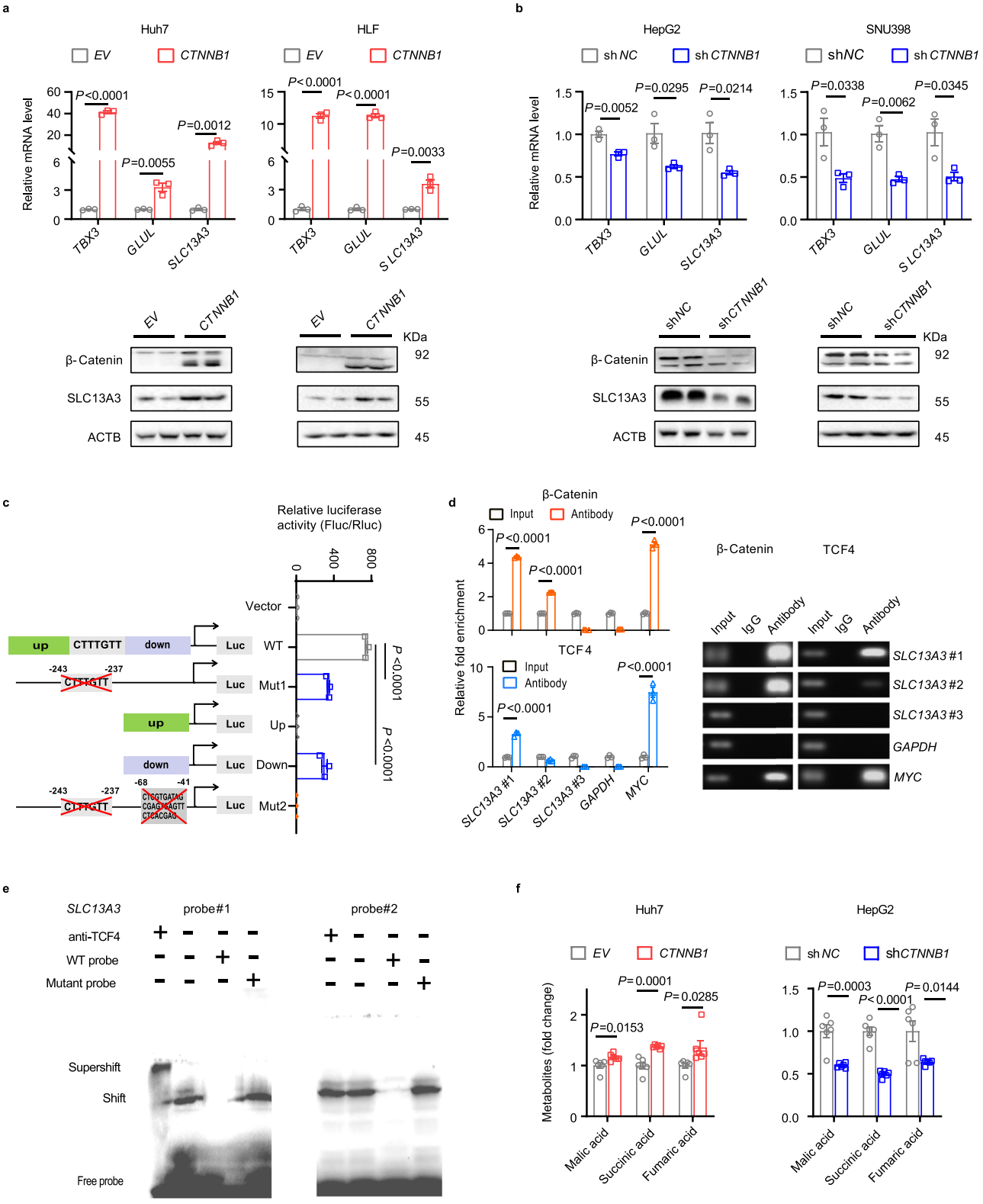


expression was significantly decreased by *SLC13A3* knockdown in both HepG2 and SNU398 cells (Supplementary Fig. 7d). qRT-PCR and western blot analyses validated the down-regulation of *MYC* in *SLC13A3*-knockdown cells (Fig. 3e). By contrast, *MYC* mRNA expression was significantly upregulated by *SLC13A3* overexpression (Supplementary Fig. 7e). It should be noted that *SLC7A5*[12] and *SLC3A2*[16] are direct target genes of c-MYC. As anticipated, *MYC* knockdown by siRNAs markedly diminished the suppression of *SLC7A5* and *SLC3A2* in *SLC13A3*-knockdown cells (Supplementary Fig. 7f). We also found that the mRNA levels of several c-MYC target genes were decreased by *SLC13A3* knockdown (Supplementary Fig. 7g). These findings suggest that c-MYC mediates the down-regulation of *SLC7A5* in *SLC13A3*-knockdown cells.

Considering that GSH was depleted in *SLC13A3*-knockdown cells and GSH depletion increases DNA methylation in hepatocytes[17], we explored whether DNA methylation contributed to the down-

**Fig. 2 | β-Catenin regulates the expression of *SLC13A3* and intracellular SLC13A3 substrates. a**, **b** mRNA expression of *TBX3*, *GLUL*, and *SLC13A3*, as well as protein levels of β-catenin and SLC13A3 in *CTNNB1*-overexpressing or *CTNNB1*-knockdown HCC cells. Huh7 and HLF cells were transfected with pT3-EF1αH plasmid (empty vector, *EV*, gray) or pT3-EF1αH plasmid containing ΔN90-β-catenin mutant fragment (*CTNNB1*, red). HepG2 and SNU398 cells were infected with shRNA lentivirus using pLKO.1 plasmid containing either scramble shRNA (negative control shRNA, sh*NC*, gray) or sh*CTNNB1* (blue) sequences. Cells were collected at 24 h for qRT-PCR and 48 h for western blot. The experiments were performed three times on different days. Each western blot represented one biological replicate (two technical repeats per group). Data are presented as the mean ± SEM ($n = 3$ independent experiments). Statistical analysis was performed using two-tailed Student's *t* test. **c** Luciferase reporter assay for the identification of β-catenin binding sites in the *SLC13A3* gene promoter region (-1.0 kb from transcription start site, TSS). A series of fragments in the *SLC13A3* promoter region were schematized. HEK293T cells were transfected with the respective promoter plasmid, pCMV-renilla, and *EV*- or *CTNNB1*-overexpressing plasmid for 24 h. Data are presented as the mean ± SEM ($n = 3$ independent experiments). Statistical analysis was performed using one-way ANOVA test. **d** Chromatin immunoprecipitation (ChIP)-PCR detection of the *SLC13A3* promoter. DNA was isolated by anti-β-catenin antibody (orange), anti-TCF4 antibody (blue), or negative control IgG (gray). Input DNA which equaled 10% total DNA samples prior to immunoprecipitation was used as positive control. DNAs were respectively amplified using *SLC13A3* promoter primers#1 (for binding site 1), #2 (for binding site 2), and #3 (spans −2100 to −2081 bp upstream of the TSS), as well as negative *GAPDH* primers and positive *MYC* primers. Data are presented as the mean ± SEM ($n = 3$ independent experiments). Statistical analysis was performed using two-tailed Student's *t* test. **e** In vitro EMSA analysis of TCF4 protein binding with two putative β-catenin binding sites in HepG2 nuclear extracts. The protein and DNA interactions were abolished by adding unlabeled wild-type probes, but could not be abrogated by mutant probes. Left panel: Adding anti-TCF4 antibody resulted in a supershift band to TCF4 protein. Right panel: No supershift band after adding anti-TCF4 antibody. SLC13A3 probe #1 was for the bind site 1, and SLC13A3 probe #2 was for the bind site 2. Each experiment was independently repeated three times. **f** Relative intracellular levels of malate, succinate, and fumarate. The data were obtained from the untargeted metabolomics in *CTNNB1*-overexpressing Huh7 cells (red) and *CTNNB1*-knockdown HepG2 cells (blue). Data are presented as the mean ± SEM ($n = 6$ independent experiments). Statistical analysis was performed using two-tailed Student's *t* test. Source data are provided as a Source Data file.

regulation of *MYC*. We found that *SLC13A3* knockdown significantly increased the expression of *DNMT1*, *DNMAT3A* and *DNMT3B* (Supplementary Fig. 8a). Knockdown of *DNMT*s by siRNAs significantly attenuated the down-regulation of *MYC* and *SLC7A5* in *SLC13A3*-knockdown cells (Supplementary Fig. 8b and 8c). Methylated DNA immunoprecipitation (MeDIP) analysis revealed a marked increase in 5-methylated-cytosine (5-mC) in the *MYC* promoter upon *SLC13A3* knockdown (Fig. 3f). Furthermore, methylation-specific PCR analysis revealed that methylation of CpG islands in the *MYC* promoter region was increased in *SLC13A3*-knockdown cells, but decreased in *SLC13A3*-overexpressing cells (Supplementary Fig. 8d). Although multiple mechanisms might be involved in *MYC* regulation, our findings suggest that SLC13A3 regulates *MYC* expression at least partially through DNA methylation.

Analyses of ChIP-seq and RNA-seq data from *Apc*-knockout and *Ctnnb1*-knockout mouse hepatocytes revealed that mouse *Slc13a3* is also a direct target gene of β-catenin[18]. Additionally, we analyzed the RNA-seq data from previously established mouse HCC models induced by various oncogenes, including AKT/β-catenin, c-Met/β-catenin, Nrf2/β-catenin, c-Myc, and AKT/c-Met (Supplementary Fig. 9a). The mRNA levels of both *Slc13a3* and *Slc7a5* were significantly elevated in mouse liver tumors induced by c-Met/β-catenin, Nrf2/β-catenin, and AKT/β-catenin, but not in AKT/c-Met driven HCC tissues. *Slc7a5*, but not *Slc13a3*, was upregulated in c-Myc-driven HCC tumor. This is not surprising because *Slc7a5* is a target gene of c-Myc. Given the upregulation of *Slc13a3* and *Slc7a5* in β-catenin-activated HCCs, we determined whether leucine is critical for β-catenin-driven hepatocarcinogenesis. We hydrodynamically injected mice with c-Met/β-catenin plasmids or AKT/β-catenin plasmids to induce liver tumors. Mice were given either a leucine deficient diet (Leu-) or leucine-supplemented drinking water (Leu + ) (Fig. 3g). In both HCC models, mice from control and Leu+ groups had to be euthanized during the treatment course, whereas mice from Leu- group survived longer (Fig. 3h). Based on liver weights and histological analysis, tumor burden and cell proliferation were higher in Leu+ group and lower in Leu- group compared to control group (Fig. 3i, j and Supplementary Fig. 9b). These findings suggest that leucine promotes β-catenin-driven hepatocarcinogenesis in mice.

## Silencing of *SLC13A3* induces autophagic ferroptosis in β-catenin-activated liver cancer cells

The in vitro effect of *SLC13A3* knockdown was determined using GOF *CTNNB1* mutant HepG2 and SNU398 cells. Both sh#1 and sh#2 significantly suppressed the proliferation and colony formation of HepG2 and SNU398 cells, which were rescued by *SLC13A3* re-expression (Fig. 4a and Supplementary Fig. 10a, b). Flow cytometry and caspase activity assays revealed that *SLC13A3* knockdown had no significant impact on apoptosis (Supplementary Fig. 10c). Necrosulfonamide (NSA), a potent necroptosis inhibitor, and Z-VAD-FMK (ZVAF), a potent apoptosis inhibitor, had little effect on the growth of *SLC13A3*-knockdown cells (Supplementary Fig. 10d). In contrast, two ferroptosis inhibitors, ferrostatin-1 (Fer-1) and liproxstatin-1 (Lip-1), significantly increased the cell viability of *SLC13A3*-knockdown cells (Fig. 4b). Ferroptosis is characterized by lipid peroxidation and iron accumulation[19]. We observed a substantial increase of lipid peroxidation in *SLC13A3*-knockdown cells using the C11-BODIPY probe or by measuring intracellular malonyl dialdehyde (MDA) (Fig. 4c). Transferrin receptor 1 (TfR1) regulates the import of iron into the cell and is considered a specific ferroptosis marker[20]. Western blot analysis revealed that *SLC13A3* knockdown increased TfR1 (Fig. 4d and Supplementary Fig. 10e).

GSH functions as a key scavenger of reactive oxygen species (ROS) and plays a crucial role in ferroptosis via GSH-glutathione peroxidase 4 (GPX4) axis[21]. Western blot analysis showed that GPX4 protein level was decreased in *SLC13A3*-knockdown cells (Fig. 4d and Supplementary Fig. 10e). Consistent with GSH depletion in *SLC13A3*-knockdown cells, we observed a significant increase in intracellular ROS (Fig. 4e and Supplementary Fig. 11a). Notably, supplementation of GSH or N-acetylcysteine (NAC) largely reversed the suppressed cell viability of *SLC13A3*-knockdown cells (Supplementary Fig. 11b). Sorafenib is the first-line drug for advanced HCC. Sorafenib can induce HCC cell ferroptosis via inhibition of SLC7A11, leading to cellular GSH depletion and elevated ROS[22]. We found that *SLC13A3* knockdown enhanced the sensitivity of liver cancer cells to sorafenib, which could be largely diminished by supplementation of GSH or NAC (Fig. 4f and Supplementary Fig. 11c). Furthermore, *SLC13A3* knockdown increased the vulnerability of cells to ferroptosis modulators of GSH-GPX4 axis (RSL3, buthionine sulfoximine, erastin) (Supplementary Fig. 11d). These results suggest that *SLC13A3* knockdown induces ferroptosis in β-catenin-activated liver cancer cells.

Ferritin is the iron storage protein critical for cellular iron homeostasis. During ferroptosis, ferritin can be degraded by autophagy, a process known as ferritinophagy[23]. ATG5 regulates the early stage of autophagosome formation. We found that *SLC13A3* knockdown markedly decreased ferritin heavy chain 1 (FTH1) and increased ATG5, suggesting the occurrence of ferritinophagy (Fig. 4d and Supplementary Fig. 10e). Notably, *ATG5* knockdown by siRNAs decreased lipid peroxidation and reversed the inhibitory growth of *SLC13A3*-knockdown cells (Supplementary Fig. 11e, f). The autophagy inhibitors chloroquine (CQ) and bafilomycin A1 (BafA1) also significantly

https://doi.org/10.1038/s41467-024-51860-2

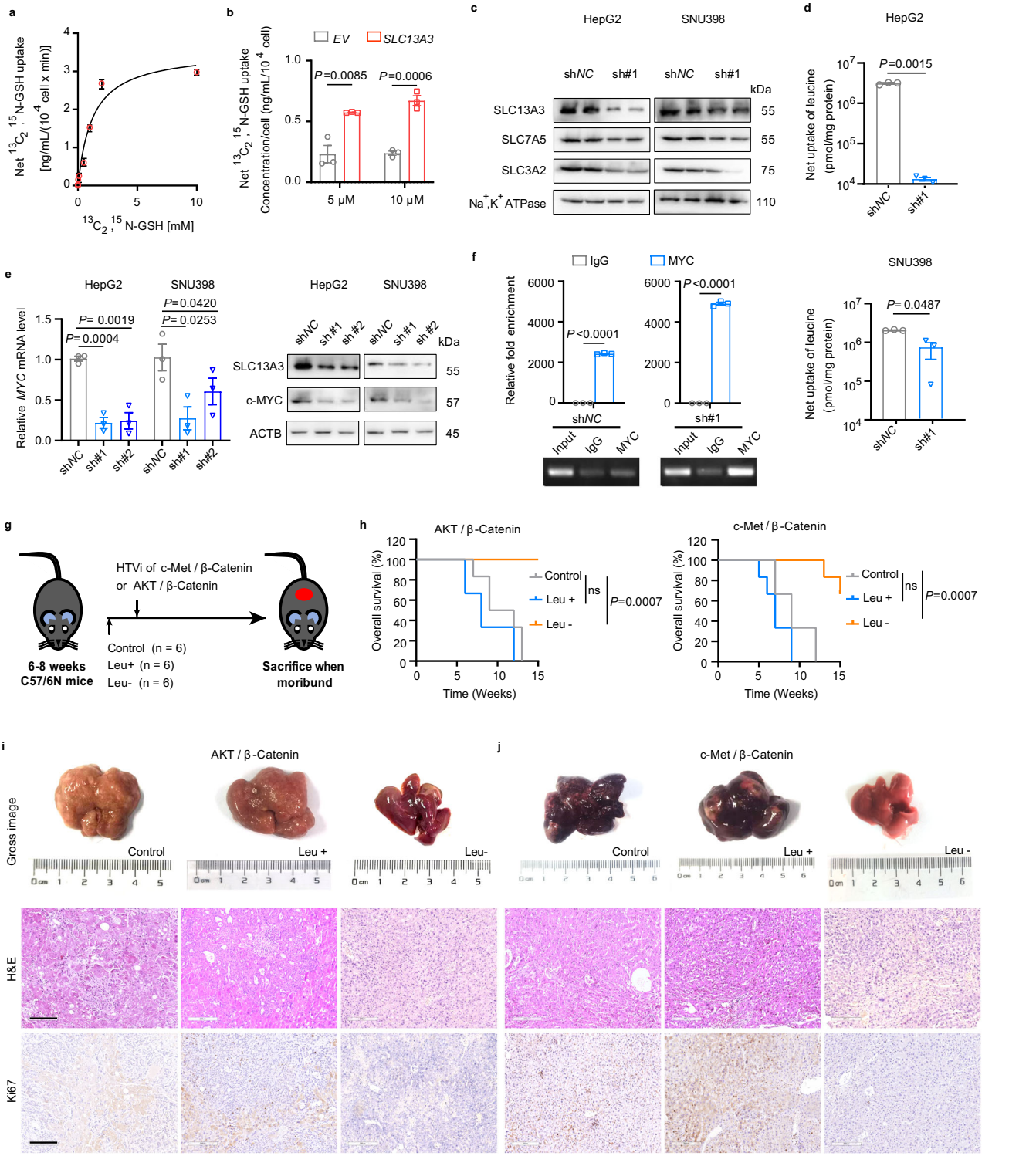


decreased lipid peroxidation in *SLC13A3*-knockdown cells (Supplementary Fig. 11g). Both western blot and fluorescence immunostaining analyses revealed that *SLC13A3* knockdown increased LC3B, a reliable biomarker of autophagosome (Fig. 4d, Supplementary Figs. 10e, 11h). By utilizing a fluorescent-tagged LC3B expression system, we demonstrated that *SLC13A3* knockdown markedly promoted autophagic flux (Fig. 4g).

mTOR serves as a master regulator of autophagy, and mTOR activation is commonly observed in β-catenin-activated liver tumors[24]. We found that *SLC13A3* knockdown significantly decreased pmTOR and its downstream effectors, pp70S6K and P62 (Fig. 4d and Supplementary Fig. 10e). Because leucine is a potent stimulator of mTOR[25] and is regulated by SLC13A3, we examined whether leucine mediated the deactivation of mTOR in *SLC13A3*-knockdown cells. Remarkably, leucine could significantly mitigate the effect of *SLC13A3* knockdown on pmTOR and its downstream proteins (Supplementary Fig. 11i). Moreover, leucine supplementation significantly restored the growth of *SLC13A3*-knockdown cells (Supplementary Fig. 11j). Additionally, we found that leucine supplementation increased pmTOR in β-catenin-driven mouse HCC tumors (Supplementary Fig. 9c). Taken together, these findings suggest that ferroptosis induced by *SLC13A3* knockdown is at least partially dependent on autophagy.

**Fig. 3 | SLC13A3 regulates intracellular glutathione and leucine in β-catenin-activated liver cancer cells. a** Cellular accumulation of $^{13}C_2$,$^{15}N$-glutathione (GSH) in HEK293 cells. HEK293-*SLC13A3* and HEK-*EV* cells were incubated with isotope-labeled GSH at concentrations from 10 nM to 10 mM for 20 min. Saturable GSH uptake was calculated using the difference of GSH accumulation in HEK293-*SLC13A3* and HEK-*EV* cells. The data were fit to a Michaelis–Menten equation. Data are presented as the mean ± SEM for a representative experiment (n = 3 independent experiments). **b** Cellular uptake of $^{13}C_2$,$^{15}N$-glutathione (GSH) (5 and 10 μM) was significantly higher in HEK-*SLC13A3* cells (red) compared to HEK293-*EV* cells (gray). Cells were incubated in the uptake buffer containing GSH for 20 min. Data are presented as the mean ± SEM (*n* = 3 independent experiments). Statistical analysis was performed using two-tailed Student's *t* test. **c** Representative western blots of SLC13A3, SLC7A5, and SLC3A2 in HepG2 and SNU398 cell. Stably control (sh*NC*) and *SLC13A3*-knockdown (sh#1) cells were established by infection with shRNA lentivirus. Blots were representative of three independent experiments (two replicates per group for each experiment). **d** Cellular uptake of 2 mM leucine in HepG2 and SNU398 cells. Stability control (sh*NC*, gray) and *SLC13A3*-knockdown cells (sh#1, blue) were incubated with 2 mM leucine for 20 min. Data are presented as the mean ± SEM (*n* = 3 independent experiments). Statistical analysis was performed using two-tailed Student's *t* test. **e** qRT-PCR and western blot analyses of *MYC* expression in HepG2 and SNU398 cells. Stably control (sh*NC*, gray) and *SLC13A3*-knockdown (sh#1, blue and sh#2, dark blue) cells were established using respective shRNA lentivirus. Data are presented as the mean ± SEM (*n* = 3 independent experiments). Statistical analysis was performed using one-way ANOVA test. Blots were representative of three independent experiments. **f** Methyl-DNA immunoprecipitation (MeDIP)-PCR detection of the *MYC* promoter methylation. DNA was immunoprecipitated with 5-methylcytosine antibody (blue) or IgG (gray), and purified according to the manufacturer's protocol. Input DNA prior to immunoprecipitation was used as the positive control. Precipitated and input DNAs were amplified using primers for the CpG islands in the *MYC* promoter region, and PCR products were visualized by gel electrophoresis. Data are presented as the mean ± SEM (*n* = 3 independent experiments). Statistical analysis was performed using two-tailed Student's *t* test. **g** Mouse study design. Mice were given a leucine-deficient diet (Leu-) or leucine-supplemented drinking water (1.5% leucine in drinking water, Leu+). Liver tumor was induced by hydrodynamic tail vein injection (HTVi) of c-Met/β-catenin plasmids or AKT/β-catenin plasmids. **h** Mice were euthanized when they developed a high burden of liver tumors. The log-rank test was used to compare overall survival between groups (Gray, control; Blue, Leu+; Orange, Leu-). ns, non-statistically significant. **i**, **j** Representative gross liver images, as well as H&E (hematoxylin-eosin) and Ki67 IHC staining images. Images were representative shown out of 6 independent mice per group. Scale bar, 200 μm. Source data are provided as a Source Data file.

## Genetic inhibition of *Slc13a3* suppresses β-catenin-driven hepatocarcinogenesis in mice

To determine the in vivo effect of *SLC13A3* knockdown, we first evaluated the impact of intratumor injection of sh*NC* or sh*SLC13A3#1* lentivirus on subcutaneous HepG2 cell xenografts in mice. qRT-PCR and IHC analyses validated the successful knockdown of *SLC13A3* by shRNA lentivirus in HepG2 xenografts (Supplementary Fig. 12a). *SLC13A3* knockdown significantly inhibited the growth of HepG2 xenografts, with a concomitant decrease in cell proliferation marker Ki67 (Supplementary Fig. 12b, c). IHC and western blot analyses showed that *SLC13A3* knockdown had no effect on apoptosis (cleaved caspase 3), but induced autophagy (decreased pmTOR, pp70S6K, and P62; increased ATG5 and LC3B) and ferroptosis (increased 4HNE, the aldehyde product of lipid peroxidation). Importantly, the ferroptosis inhibitor liproxstatin-1 significantly reversed the growth inhibitory effect of *SLC13A3* knockdown on HepG2 xenografts (Fig. 5a).

Next, we determined the impact of *Slc13a3* knockdown on β-catenin-driven hepatocarcinogenesis in mice. We first showed that hydrodynamic injection of the sh*Slc13a3*#1 and sh*Slc13a3*#2 lentivirus mixture successfully decreased *Slc13a3* expression in mouse liver (Supplementary Fig. 13a). Subsequently, mice were subject to hydrodynamical injection of the shRNA lentivirus mixture together with c-Met/β-catenin plasmids or AKT/β-catenin plasmids to induce liver tumor (Fig. 5b). Staring from 7- or 8-weeks post-injection, all mice treated with control shRNA lentivirus (sh*NC*) exhibited large abdominal masses and eventually became moribund, while mice injected with sh*Slc13a3* lentivirus appeared healthy as of 15 weeks post-injection (Fig. 5c, d). Consistently, sh*Slc13a3*-treated mice had significantly lower tumor burden than sh*NC*-treated mice (Figs. 5e and 5f). Finally, we investigated the molecular mechanisms underlying the tumor-suppressing effect of sh*Slc13a3* lentivirus. The high immunoactivity of MYC-tagged β-catenin (MYC) in c-Met/β-catenin-driven liver tumors and HA-tagged myr-AKT1 (HA) in AKT/β-catenin-driven liver tumors implied their origin from the transfected cells (Fig. 5e, f). The immunoactivity of Ki67 and 4HNE revealed that *Slc13a3* knockdown decreased tumor cell proliferation and increased ferroptosis. As anticipated, SLC13A3 and SLC7A5 protein levels were increased in β-catenin-driven liver tumors of sh*NC*-injected mice, but were decreased in sh*Slc13a3*-injected mice (Supplementary Fig. 13b). Consistently, *Slc13a3* knockdown decreased intracellular GSH and leucine in β-catenin-driven mouse liver tumors (Supplementary Fig. 13c). Furthermore, western blot analysis revealed that *Slc13a3* knockdown did not significantly altered apoptosis (cleaved caspase 3), but induced autophagy (decreased pmTOR and P62, increased ATG5 and LC3B) and ferroptosis (increased TfR1) (Supplementary Fig. 13b). These findings suggest that *Slc13a3* knockdown by shRNA lentivirus impedes β-catenin-driven hepatocarcinogenesis.

To further validate the role of SLC13A3, we utilized a CRISPR/Cas9 lentivirus system to knockout *SLC13A3* in human HCC cells (Supplementary Fig. 14a, b). As anticipated, *SLC13A3* deficiency markedly inhibited cell viability and colony formation of HepG2 and SNU398 cells, which could be rescued by *SLC13A3* re-expression (Fig. 6a, b). Western blot analysis revealed that *SLC13A3* deficiency decreased leucine transporters SLC7A5 and SLC3A2, and induced ferroptosis markers (increased TfR1, decreased FTH1 and GPX4) (Fig. 6c). Supplementation with leucine, GSH or NAC could significantly increase the viability of *SLC13A3* deficient cells (Supplementary Fig. 14c). Furthermore, *SLC13A3* deficiency decreased mRNA expression of *MYC*, without significantly altering GSH synthetic genes (Supplementary Fig. 14d). Subsequently, we utilized a CRISPR/Cas9 adeno-associated virus 8 (AAV8) system to knockout *Slc13a3* in mouse hepatocytes (Supplementary Fig. 14e, f). Two weeks after AAV8 virus injection, c-Met/β-catenin plasmids or AKT/β-catenin plasmids were injected to induce HCC in mice (Fig. 6d). While AAV8-sg*Slc13a3* could not completely deplete SLC13A3 protein in mouse liver, it significantly prolonged the survival of β-catenin-driven HCC mice, with reduced liver tumor burden (Fig. 6e, f). Liver histological and IHC analysis revealed that AAV8-sg*Slc13a3* substantially decreased the cell proliferation marker Ki67 (Fig. 6g). It should be noted that the experimental procedures were different between shRNA knockdown and sgRNA knockout mouse studies. We hydrodynamically co-injected the shRNA virus mixture along with β-catenin plasmids to induce liver tumors, while sgRNA was injected two weeks prior to the hydrodynamic injection of β-catenin plasmids. Taken together, these findings support the therapeutic targeting potential of SLC13A3 in β-catenin-driven hepatocarcinogenesis.

## The SLC13A3 inhibitor ACA suppresses the growth of human HCC cells and prevents β-catenin-driven hepatocarcinogenesis in mice

N-(*p*-amylcinnamoyl) anthranilic acid (ACA) has been used as an inhibitor of SLC13A3 to explore its functions[26,27]. We found that ACA markedly inhibited cell viability and colony formation of HepG2 and SNU398 cells in a dose-dependent manner (Supplementary Fig. 15a). ACA dose-dependently decreased mRNA and protein levels of *SLC13A3* (Supplementary Fig. 15b). The inhibitory effect of ACA on cell viability

https://doi.org/10.1038/s41467-024-51860-2

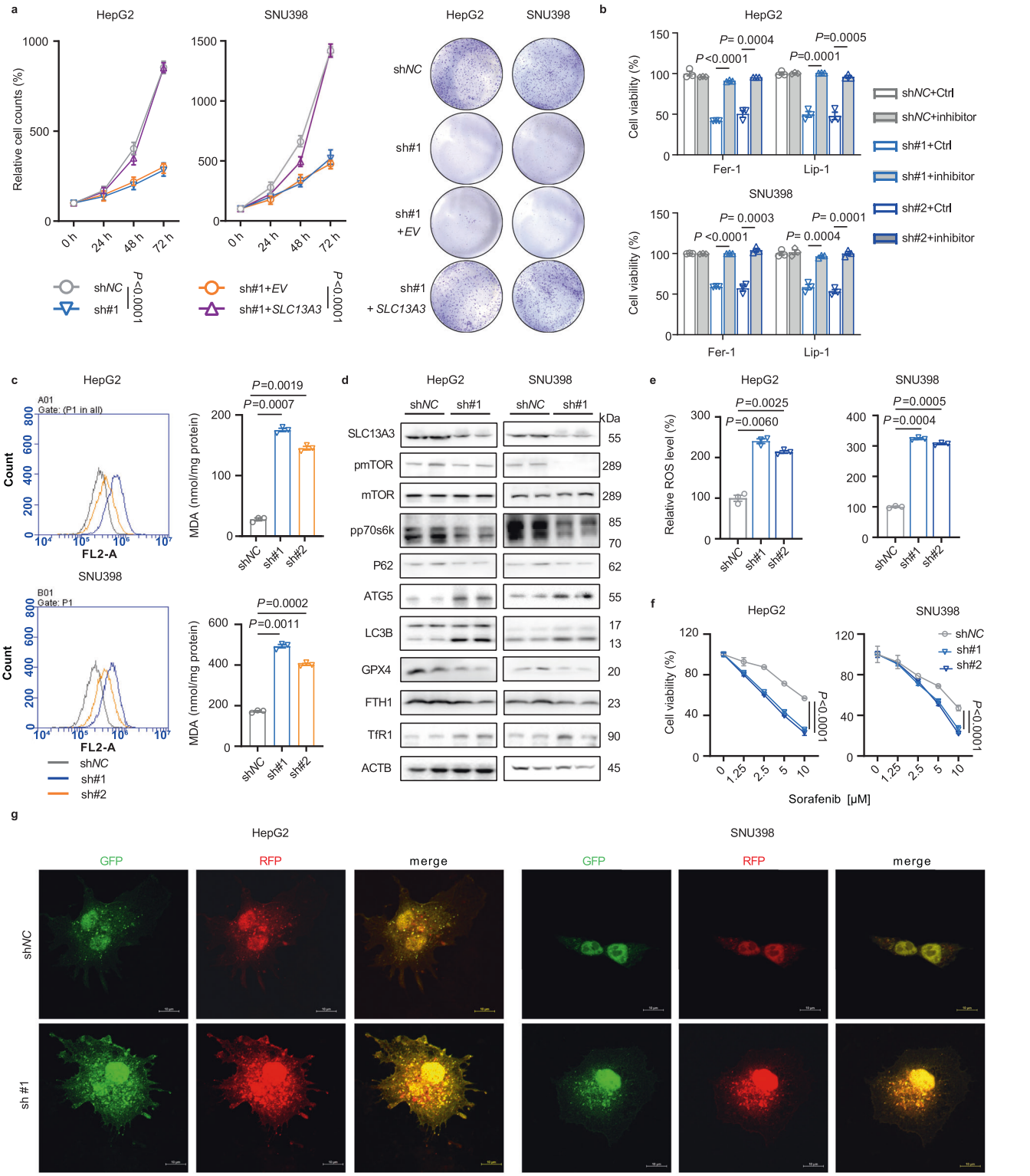


could largely be reversed by forced expression of *SLC13A3* (Supplementary Fig. 15c). Although ACA also inhibits SLC13A2 and SLC13A5[28], it is noteworthy that *SLC13A2* expression is low in liver tissues[28]. Consistently, HPA analysis revealed almost undetectable *SLC13A2* expression in liver cancer cells (Supplementary Fig. 15d). This indicates that SLC13A2 is unlikely the target of ACA in suppressing HCC cell viability. Interestingly, while *SLC13A5* mRNA was highly expressed in HepG2 and Huh7 cells, it was almost undetectable in other HCC cells, including those with β-catenin activation (Supplementary Fig. 15d). The SLC13A5 specific inhibitor PF-06761281[29] had no effect on cell viability of HepG2 cells, and *SLC13A5* overexpression did not reverse the inhibitory effect of ACA on cell viability (Supplementary Fig. 15e, f). This suggests that SLC13A5 is also not the target for ACA in suppressing HCC cell viability. Besides the SLC13A transporters, ACA has been reported to inhibit PLA2, TRPM2, and AP2M1[30]. HPA analysis revealed that *TRPM2* expression was almost undetectable in liver cancer cells (Supplementary Fig. 15d). While inhibition of PLA2[31] and AP2M1[32] has been shown to suppress autophagy, ACA induced autophagy in HCC cells (Supplementary Fig. 16). Furthermore, overexpression of *PLA2*, *TRPM2*, and *AP2M1* did not inhibit ACA cytotoxicity in HCC cells (Supplementary

**Fig. 4 | *SLC13A3* knockdown induces autophagic ferroptosis. a** Growth curves and colony formation of HepG2 and SNU398 cells. Stably control (sh*NC*, gray) and *SLC13A3*-knockdown (sh#1, blue) cells were established using shRNA lentivirus. For re-expression study, cells were transfected with *EV*- (orange) or *SLC13A3*-over-expressing (purple) plasmid for 24 h. Cell viability was determined at the indicated time. Colony formation was measured by incubating cells in 12-well plates for 2 weeks. Data are presented as the mean ± SEM (n = 3 independent experiments). Statistical analysis was performed using one-way ANOVA test. **b** Cell viability of HepG2 and SNU398 cells. Stably control (sh*NC*, gray bar) and *SLC13A3*-knockdown (sh#1, blue bar and sh#2, dark blue bar) cells were treated with 1 μM ferrostatin-1 (Fer-1) or 10 μM liproxstatin-1 (Lip-1) for 48 h. Data are presented as the mean ± SEM (*n* = 3 independent experiments). Statistical analysis was performed using one-way ANOVA test. **c** Intracellular fluorescence of C11-BODIPY probe and malonyl dialdehyde (MDA) levels in HepG2 and SNU398 cells. Stably control (sh*NC*, gray) and *SLC13A3*-knockdown (sh#1, blue and sh#2, orange) cells were incubated with 2% FBS-PBS containing 5 μM C11-BODIPY for 30 min, and the fluorescence was determined using flow cytometric analysis. Data are presented as the mean ± SEM (*n* = 3 independent experiments). Statistical analysis was performed using one-way ANOVA test. **d** Representative western blots of HepG2 and SNU398 cells (*n* = 3 independent experiments). Stably control (sh*NC*) and *SLC13A3*-knockdown (sh#1) cells were established using shRNA lentivirus. **e** ROS levels in HepG2 and SNU398 cells. Stably control (sh*NC*, gray bar) and *SLC13A3*-knockdown (sh#1, blue bar and sh#2, dark blue bar) cells were incubated with 10 μM DCFH-DA for 30 min, and the fluorescence was measured. Data are presented as the mean ± SEM (n = 3 independent experiments). Statistical analysis was performed using one-way ANOVA test. **f** Cell viability of *SLC13A3*-knockdown (sh#1, blue curve and sh#2, dark blue curve) HepG2 and SNU398 cells in the presence of sorafenib at the indicated concentrations (0, 1.25, 2.5, 5, 10 μM) for 48 h. Data are presented as the mean ± SEM (*n* = 3 independent experiments). Statistical analysis was performed using one-way ANOVA test. **g** Autophagosome formation was measured using mRFP-GFP-LC3 puncta in HepG2 and SNU398 cells (*n* = 3 independent experiments). Stably control (sh*NC*) and *SLC13A3*-knockdown (sh#1) cells were transfected with 1 μg mRFP-GFP-LC3 plasmid for 24 h, and imaged using confocal microscopy (GFP, green; RFP, red; merge, yellow). Source data are provided as a Source Data file.

Fig. 15g), nor did ACA treatment alter their mRNA expression (Supplementary Fig. 15h). Although we cannot completely rule out the potential "off-target" effects of ACA, these findings suggest that ACA inhibits HCC cell viability, at least partially, via SLC13A3.

To determine whether ACA exerts similar effects as *SLC13A3* genetic inhibition, we characterized the potential mechanisms underlying ACA-mediated cell growth inhibition. ACA had no significant effect on apoptosis (Supplementary Fig. 16a). The growth inhibitory effect of ACA could be rescued by inhibitors of autophagy (bafilomycin A1 and chloroquine) and ferroptosis (liproxstatin-1 and ferrostatin-1), but not by inhibitors of necrosis (NSA) or apoptosis (Z-VAD-FMK) (Supplementary Fig. 16b). ACA-induced ferroptosis was further evidenced by elevated lipid ROS (C11-BODIPY fluorescence) (Supplementary Fig. 16c). Western blot analysis showed that ACA induced autophagy (decreased pmTOR and P62, increased ATG5 and LC3B) and ferroptosis (decreased FTH1 and increased TfR1) biomarkers in a dose-dependent manner (Fig. 7a*)*. Additionally, ACA showed a synergistic effect with sorafenib on cell viability and colony formation of HepG2 and SNU398 cells (Fig. 7b and Supplementary Fig. 16d).

Next, we investigated the in vivo effect of ACA in mice. ACA did not cause apparent toxicity in normal C57BL/6 N or BALB/C nude mice (Supplementary Fig. 16e). ACA (30 mg/kg, i.p., every other day) effectively suppressed the growth of subcutaneous HepG2 xenografts in BALB/C nude mice, showing a synergistic effect with sorafenib (Fig. 7c). Western blot and IHC analysis revealed that ACA induced autophagy and ferroptosis in HepG2 xenografts (Fig. 7d and Supplementary Fig. 16f). To further investigate the impact of ACA on β-catenin-driven hepatocarcinogenesis, ACA (30 mg/kg, every other day) was administered intraperitoneally to C57BL/6 N mice starting from the 4$^{th}$ week post injection of c-Met/β-catenin and AKT/β-catenin plasmids (Fig. 7e). While all vehicle-treated mice had to be euthanized during the experimental course, ACA-treated mice appeared to be healthy even after 15 weeks post plasmid injection (Fig. 7f). IHC and western blot analysis indicated that ACA induced autophagy (increased ATG5 and LC3B; decreased pmTOR and P62) and ferroptosis (increased 4HNE and TfR1; decreased FTH1) (Fig. 7g and Supplementary Fig. 16g). These findings indicate that ACA exerts similar effects to genetic inhibition of *SLC13A3* on β-catenin-activated liver cancer.

## Discussion

While many direct downstream targets of β-catenin have been identified, only a limited number of them have been suggested as potential targetable genes for treating β-catenin-activated liver cancer. Glutamine synthetase (GS) is a liver-specific downstream target of β-catenin, and GS-mediated glutamine synthesis activates mTORC1 in *CTNNB1*-mutated HCC[24]. However, mTOR is not a direct target of β-catenin and could be modulated by multiple cascades. Consequently, the mTOR inhibitor everolimus only shows limited efficacy against advanced HCC[33]. Given the significance of SLC transporters as valuable targets for drug development, we show that inhibition of *SLC13A3*, a direct downstream target gene of β-catenin, effectively impedes β-catenin-driven hepatocarcinogenesis (Fig. 7h).

The TCA cycle intermediates have a profound impact on cancer development[34]. Three SLC13 family members, namely SLC13A2, SLC13A3, and SLC13A5, are capable of transporting the TCA cycle metabolites. Among them, SLC13A3 and SLC13A5 are highly expressed in the liver[7]. Previous studies suggest that SLC13A5 regulates the uptake of citrate in liver cancer, and its inhibition suppresses the growth of HepG2 and Huh7 cells[35,36]. However, our data show that β-catenin activation has no significant impact on *SLC13A5* expression (Supplementary Fig. 17a). Furthermore, both mRNA and protein levels of *SLC13A5* are significantly down-regulated in human HCCs (Supplementary Fig. 17b, c). These findings suggest that SLC13A5 is not an ideal direct therapeutic target for liver cancer treatment. In contrast, we show that β-catenin activation upregulates SLC13A3, leading to an increase of intracellular SLC13A3 substrates (succinate and fumarate) in liver cancer cells. Interestingly, the accumulation of succinate or fumarate, caused by mutations in succinate dehydrogenase (SDH) or fumarate hydratase (FH), has been implicated in tumor development and progression[34]. Future studies are needed to determine whether SLC13A3-mediated accumulation of succinate and fumarate can drive oncogenic cascades in β-catenin-activated liver cancer.

Although inconsistent findings have been reported on the blood level of leucine in HCC patients[37], leucine appears to be upregulated in HCC tumor tissues[38], particularly in the NFALD type HCC[39]. Coincidently, aberrated Wnt/β-catenin signaling is implicated in the progression from NFALD to HCC[40]. Leucine supplementation has been shown to promote bladder carcinogenesis in rats[41,42], and increase pancreatic tumor growth in xenografted mice[43]. However, the in vivo effect of leucine supplementation on HCC is yet to be fully understood. Leucine is one of the branched-chain amino acids (BCAAs), which have demonstrated controversial impacts on HCC tumorigenesis and progression. In two clinical studies, oral administration of BCAAs prevents hepatocarcinogenesis in patients with cirrhosis[44] and reduces early recurrence after hepatic resection in HCC patients[45]. In contrast, Ericksen et al. reported that BCAA supplementation markedly increases the incidence and metastasis of DEN-induced liver tumors in mice[46]. Nevertheless, we show that SLC13A3 is a key regulator of intracellular leucine, and identify a promoting effect of leucine on β-catenin-driven hepatocarcinogenesis in mice.

https://doi.org/10.1038/s41467-024-51860-2

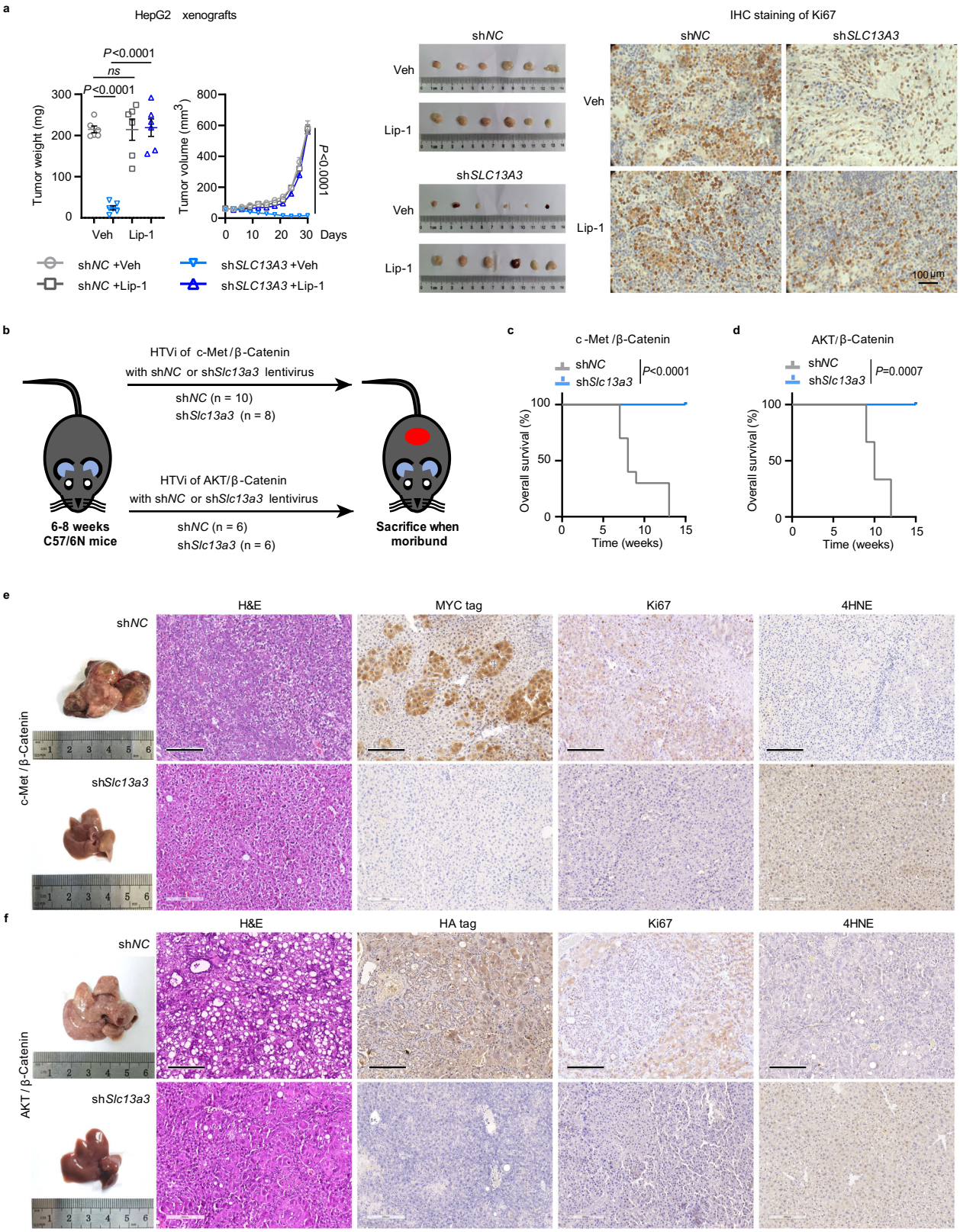


GSH is the most abundant thiol-containing compound in mammalian cells and has a primary role in regulating the antioxidant stress and various signal transduction reactions. GSH dysregulation has been implicated in tumor initiation, progression and treatment response[47]. GSH is particularly concentrated in the liver (~10 mM), which is the major site of GSH synthesis. Notably, much of the GSH synthesized inside hepatocytes is constantly exported into liver sinusoids[48]. Because GSH is rapidly metabolized in the circulation leading to low plasma GSH levels (~10 μM), the re-uptake of GSH from the sinusoidal space into hepatocytes is highly questionable. However, it should be noted that the tumor microenvironment is totally different from normal tissue. For example, the extracellular pH in tumors including liver cancer is usually acidic (pH=5.8-6.8)[49]. It is reported that the acidic pH could dramatically alter the metabolism of GSH[50]. Therefore, the

**Fig. 5 | *Slc13a3* knockdown impedes β-catenin-driven hepatocarcinogenesis in mice. a** Tumor weights, tumor volumes, representative gross tumors and Ki67 IHC staining images of HepG2 xenografts in BALB/C nude mice. Knockdown of *SLC13A3* was achieved by intratumor injection with shRNA lentivirus (sh*SLC13A3* #1) (Gray curve, sh*NC* group; Blue curve, sh*SLC13A3* group). After shRNA lentivirus treatment, mice were administered either vehicle or the ferroptosis inhibitor liproxastatin-1 (Lip-1,10 mg/kg, i.p., every two days). Data are presented as the mean ± SEM ($n = 6$ independent mice per group). Statistical analysis was performed using one-way ANOVA test. **b** Study design of β-catenin-induced HCC mouse models. Mice were subjected to hydrodynamic tail vein injection (HTVi) of c-Met/β-catenin plasmids or AKT/β-catenin plasmids, along with sh*NC* (negative control shRNA) or a mixture of two sh*Slc13a3* lentiviruses (sh*Slc13a3* #1 and sh*Slc13a3* #2). **c**, **d** Survival curves. Mice were euthanized when they developed a high burden of liver tumors (Gray, sh*NC* group; Blue, sh*Slc13a3* group). The log-rank test was used to compare overall survival between groups. **e**, **f** Representative gross liver images, as well as H&E (hematoxylin-eosin) and IHC staining images of c-Met/β-catenin-driven and AKT/β-catenin-driven mouse liver tumors with or without *Slc13a3* lentivirus injection (sh*NC* vs sh*Slc13a3*). Images were representative shown out of at least 6 independent mice per group. Scale bar, 200 μm. Source data are provided as a Source Data file.

potential role of sinusoidal GSH re-uptake in liver cancer development could not be excluded. In this study, we show that SLC13A3 is a low-affinity GSH transporter and can transport GSH at physiologically concentrations. *SLC13A3* knockdown not only impedes the uptake of GSH from the culture medium, but also decreases GSH precursor amino acids through c-MYC-SLC7A5 signaling. Consequently, SLC13A3 is identified as a key regulator of intracellular GSH in β-catenin-activated liver cancer cells.

The induction of ferroptosis presents a promising strategy for liver cancer treatment. Sorafenib, a first-line drug for patients with advanced HCC, is recognized as an inducer of ferroptosis. Combining sorafenib with agents that increase ROS would enhance its antitumor effect on HCC. Multiple compounds, including diclofenac[51], terandrine[52], and artesunate[53], have been demonstrated to augment sorafenib action in HCC cells by elevating ROS. In our study, we demonstrate that SLC13A3 inhibition is an effective approach to deplete GSH, increase ROS, and enhance sorafenib sensitivity in β-catenin-activated liver cancer cells. Our findings support the involvement of the GSH-GPX4 axis in inducing ferroptosis in *SLC13A3*-knockdown cells. However, other regulators may also play a role in *SLC13A3*-mediated ferroptosis. For instance, *SLC13A3* knockdown increased sensitivity of HCC cells to auranofin (AF), an inhibitor of thioredoxin reductase (Supplementary Fig. 11d). Interestingly, the activation of the Wnt/β-catenin signaling has been shown to promote ferroptosis resistance in various cancer cells[54]. The β-catenin inhibitor ICG-001 significantly enhances sorafenib sensitivity in multiple liver cancer cell lines[55]. Our findings suggest that targeting the downstream effector of β-catenin, such as SLC13A3, can also increase the sensitivity to ferroptosis inducers in β-catenin-activated HCCs.

In conclusion, our study highlights the importance of SLC13A3 in the regulation of ferroptosis in β-catenin-activated liver cancer. It is important to clarify that we do not imply that only β-catenin-activated liver cancer is sensitive to SLC13A3 inhibition. Rather, we believe that β-catenin-activated liver cancer will exhibit specific sensitivity to SLC13A3 inhibition. Inhibition of SLC13A3 is a promising strategy for targeting the β-catenin signaling in liver cancers without causing significant adverse effects.

## Methods

### Ethical statement

All protocols for animal studies were approved by Animal Ethics Committee at the Institute of Radiation Medicine of the Chinese Academy of Medical Sciences (CAMS) (No.IRM-DWLL-2021177). Mice were monitored daily for signs of HCC progression. Moribund animals (the subcutaneous tumor reached a size larger than 2 cm in diameter or liver weight reached 1/10 of body weight) were sacrificed. Animal handling was in accordance with ARRIVE Guidelines 2.0 and CAMS Guide for Care and Use of Laboratory Animals. Human hepatocellular carcinoma tissue microarrays were obtained from Outdo Biotech Inc. (Shanghai, China) with the approved protocol (No. YB M-05-02). Informed consent was obtained from patients before tissue collection.

### Plasmid constructs

The following plasmids were obtained from Addgene (Cambridge, MA, USA): mRFP-GFP-LC3 (#21074), pT3-EF1αH N90-beta-catenin with MYC tag (#86499), pT3-myr-AKT-HA with HA tag (#31789), pT3-EF1αH c-Met (#86498), pCMV/sleeping beauty transposase (SB) (#34879), and 3rd generation lentiviral packaging plasmids (pMDLg/pRRE #12251, pMD2.G #12259, pRSV-Rev #12253). The shRNA sequences (Supplementary Table 1) were synthesized by Genewiz (Tianjin, China) and inserted into pLKO.1-TRC vector (Addgene #10879). The CDS regions of genes were amplified using cDNA templates from human HepG2 cell line or mouse liver tissue, and cloned into pLenti-puro vector (Addgene #39481). The primers for CDS amplification were listed in Supplementary Table 2. All constructs were validated by sequencing.

### Reagents and chemicals

Bafilomycin A1 (BafA1), chloroquine (CQ), necrosulfonamide (NSA), Z-VAD-FMK (ZVAF), ferrostatin-1 (Fer-1), liproxstatin-1 (Lip-1), and erastin were purchased from Selleck Chemicals (Houston, TX, USA). PF-06761281, DL-buthionine-(S,R)-sulfoximine (BSO), RSL3, and auranofin (AF) were obtained from MedChemExpress LLC (Shanghai, China). Leucine, glutathione (GSH), and N-acetyl-L-cysteine (NAC) were purchased from Solarbio Life Science (Beijing, China). Glutathione-(glycine-$^{13}C_2$,$^{15}N$) was purchased from Sigma-Aldrich (St. Louis, MO). N-(p-amylcinnamoyl) anthranilic acid (ACA) and sorafenib for animal studies were synthesized by SuperLan Chemical Co., Ltd. (Shanghai, China). $^{14}$C-Succinic acid (Moravek, Cat#MC 238) was purchased from Moravek Biochemicals (Brea, CA, USA).

### Cell culture

HepG2 (ATCC, HB-8065) and Huh7 (NICR, 1101HUM-PUMC000679) cell lines were obtained from National Infrastructure of Cell line Resource (Beijing, China). Human liver hepatocellular carcinoma cell line Huh6 (TCHu181), SK-HEP-1 (TCHu109), and human embryonic kidney cell line HEK293 (ATCC, CRL-1573) were obtained from Cell Resource Center of Shanghai Institutes for Biological Sciences (Shanghai, China). SNU398 cell line (ATCC, CRL-2233) was obtained from Guangzhou Cellcook Biotech Co., Ltd. (Guangdong, China). Li-7 cell line was bought from Wuhan Boster Biological Engineering Co., Ltd. (Wuhan, China). SNU449 (ATCC, CRL-2234) and HLF cells were kindly gifts from Dr. Xinhua Song at Capital Medical University (Beijing, China). SNU398, SNU449, and Li-7 cells were maintained in RPMI-1640 medium (Biological Industries, Kibbutz Beit-Haemek, Israel) supplemented with 10% fetal bovine serum (FBS, Biological Industries, Kibbutz Beit-Haemek, Israel) and 1% penicillin/streptomycin (P/S, Biological Industries, Kibbutz Beit-Haemek, Israel). SK-HEP-1 cells were cultured in MEM medium (Biological Industries, Kibbutz Beit-Haemek, Israel) supplemented with 10% FBS and 1% P/S. Other cell lines were maintained in Dulbecco's Modified Eagle's Medium (DMEM, Biological Industries, Kibbutz Beit-Haemek, Israel) with 10% FBS and 1% P/S. All cell lines were maintained in 37 °C with 5% $CO_2$.

### Lentivirus infection

A four-plasmid system was used for lentivirus production. HEK293T cells ($2.5\times10^6$) were plated in 60 mm dishes pre-coated with poly-D-lysine (0.1 mg/mL dissolved in sterilized water) (Sigma-Aldrich, St. Louis, MO). After 24 h, HEK293T cells were starved with 3 mL of opti-MEM (Gibco, Thermo Fisher Scientific, Gaithersburg, MD, USA)

https://doi.org/10.1038/s41467-024-51860-2

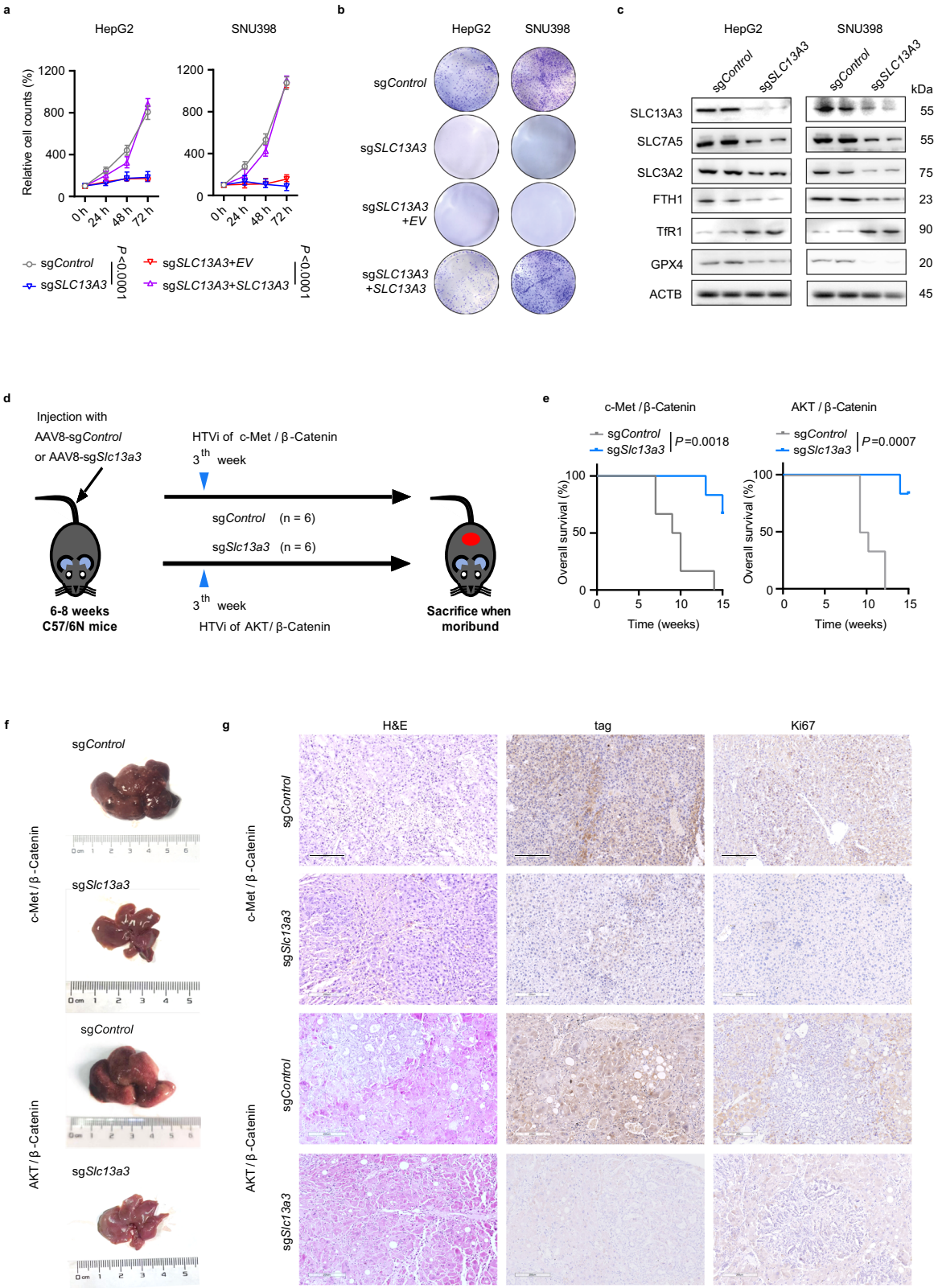


for 4 h. Three plasmids (1 μg pMDLg/pRRE, 1 μg pMD2.G, and 1 μg pRSV-Rev) and 3 μg pLKO.1 plasmid (the indicated shRNA plasmid) or pLenti-puro plasmid (overexpressing plasmid) were mixed in 250 μL of opti-MEM. Next, 18 μL of transfection reagent PEI (Polyethyleneimine, 1 mg/mL dissolved in sterilized water, pH 7.0 adjusted with 1 M NaOH) (Sigma-Aldrich, St. Louis, MO) was mixed with 250 μL of opti-MEM. After 5 min incubation at room temperature, plasmid mixture and PEI mixture were mixed and incubated at room temperature for additional 20 min, and then added into HEK293T cell culture for transfection.

After 16 h transfection, HEK293T cell culture medium was changed to DMEM with 10% FBS containing no antibiotics. Lentivirus medium was collected after 48 h and 72 h, respectively, and then centrifuged at 112 × *g* for 5 min to remove cell debris. The lentivirus medium was concentrated in 5 × PEG8000 (Beijing Dingguo Changsheng Biotechnology Co.,

**Fig. 6 | *Slc13a3* deficiency inhibits the growth of β-catenin-activated HCCs. a** Cell viability of HepG2 and SNU398 cells. Stably control (sg*Control*, gray curve) and *SLC13A3*-deficient (sg*SLC13A3*, blue curve) cells were established by infection with CRISPR/Cas9 sg*Control* or sg*SLC13A3* lentivirus, respectively. For re-expression study, sg*Control* and sg*SLC13A3* cells were transfected with empty vector (*EV*, red)- or *SLC13A3*-overexpressing (purple) plasmids for 24 h. Cell viability was determined at the indicated time points. Data are presented as the mean ± SEM ($n = 3$ independent experiments). Statistical analysis was performed using one-way ANOVA test. **b** Colony formation was measured by incubating infected cells in 12-well plates for 2 weeks. **c** Representative western blots of SLC13A3, SLC7A5, SLC3A2, FTH1, TfR1, and GPX4 in sg*Control* and sg*SLC13A3* HepG2 and SNU398 cells ($n = 3$ independent experiments, two replicates per group). **d** Mouse study design. Mice were intravenously injected with AAV8-CRISPR/Cas9 sg*Control* or sg*Slc13a3* virus. After two weeks, mice were subjected to hydrodynamic tail vein injection (HTVi) of c-Met/β-catenin plasmids or AKT/β-catenin plasmids to induce liver tumors. **e** Mice were euthanized when they developed a high burden of liver tumors (sg*Control*, gray curve; sg*Slc13a3*, blue curve). The log-rank test was used to compare overall survival between groups. **f** Gross images of liver tumors in mice with or without sg*Slc13a3* injection. Images were representative shown out of 6 independent mice per group. **g** Representative images of H&E and IHC staining. Images were representative shown out of 6 independent mice per group. Scale bar, 200 μm. Source data are provided as a Source Data file.

Beijing, China) overnight. After centrifuging at 4000 × *g* for 20 min, sediment was resuspended in phosphate-buffered saline (PBS, 1/10 of original volume) and stored at -80 °C.

For cell infection, lentivirus medium was directly added into cell culture (1:1 with fresh medium without antibiotics) for 24 h. Stably gene knockdown cells (HepG2-sh*NC* and HepG2-sh*SLC13A3* cell lines, SNU398-sh*NC* and SNU398-sh*SLC13A3* cell lines) or overexpressing cells (HEK293-*EV* and HEK293-*SLC13A3* cell lines) were established by infection with respective lentivirus, and selected in the presence of 2 μg/mL puromycin (Sigma-Aldrich, St. Louis, MO) for 10 days. For hydrodynamic tail veil injection in mice, lentivirus was filtered with a 0.45 μm membrane filter (Millipore Corporation, Burlington, MA) before injection.

### Gene knockout by CRISPR/Cas9-sgRNAs

The sgRNA expression plasmids targeting human *SLC13A3* (sgRNA: GATGGTGACAATAGCCACGC) or mouse *Slc13a3* (sgRNA: GGAAGGAGGATGAATATCGT) were constructed by ligating the corresponding annealed guide oligonucleotides to pLenti-U6-sgRNA-EFFS-spCas9-P2A-Puro plasmid co-expressing the Cas9. Lentiviruses were packaged as mentioned above. Human HEK293 and mouse N2A cells were infected with lentivirus, and genomic DNAs were extracted. PCR primers (Human: F-CCCCTCTTTGGTCAAGTCCC, R-GGAGAAGCAGGAAGGACCAC; Mouse: F-CACTGCACGTATGAGGAATGC, R-TCCACTCTCCCTCTGCCTTT) were designed to span about 500 bp at the upstream and downstream of the gRNA target site, respectively. DNA was amplified with PCR primers, and the PCR products were subjected to sequencing.

After sgRNA knockout effects were validated, human sg*Control* and sg*SLC13A3* lentiviruses were packaged using a four-plasmid system as mentioned above. HepG2 and SNU398 cells were infected with sg*Control* and sg*SLC13A3* lentivirus, and stably cells were selected in the presence of 2 μg/mL puromycin for 2 weeks. Western blot assay was used to validate the knockout effects. For the mouse study, mouse sg*Control* and sg*Slc13a3* sequences were constructed into pAV-TBG-SaCas9-U6-gRNA plasmid. Adeno-Associated Virus serotype 8 (AAV8) were packaged in HEK293 cells, and then injected into mice intravenously with $5 \times 10^{11}$ vg/mL (diluted with sterile PBS). After two weeks, mouse livers were isolated, and western blot assay was used to validate the knockout effect.

### Gene knockdown by siRNA reverse transfection

Before plating cells, 1 μL of siRNA (6 μM dissolved in DEPC water) (Gene Pharma, Shanghai, China) was diluted into 50 μL of opti-MEM, and meanwhile 1 μL of Lipofectamine™ RNAiMAX transfection reagent (Thermo Fisher Scientific, Gaithersburg, MD, USA) was diluted in 50 μL of opti-MEM. After incubation at room temperature for 5 min, the transfection reagent mixture was added into siRNA mixture, and incubated at room temperature for additional 20 min. Cells ($1 \times 10^5$/mL) were trypsinized, pelleted, resuspended in 500 μL of DMEM or RPMI-1640 medium (without antibiotics), and seeded into a 24-well plate. The siRNA transfection mixture was then added into each well, and mixed well by rocking the plate back and forth.

To determine the role of DNMTs in regulating *c-MYC* and *SLC7A5*, stably *SLC13A3*-knockdown HepG2 and SNU398 cells were transfected with siRNAs of *DNMT1/3A/3B* for 6 h, followed by culturing in complete medium.

For lipid peroxidation detection, stably *SLC13A3*-knockdown HepG2 and SNU398 cells were transfected with *ATG5* siRNAs for 6 h, followed by culturing in complete medium. The RNA and proteins were extracted from cells after siRNA transfection for 24 h and 48 h, respectively. The siRNA sequences were listed in Supplementary Table 3. Each experiment was repeated three times.

### Cell viability assay and relative cell number assay

Cells were seeded in 96-well plates (5000 cells/well) for the indicated treatments. Cell viability was determined by adding 0.1 mg/mL (final concentration) AlamarBlue cell viability reagent (Sigma-Aldrich, St. Louis, MO) into cell culture medium for 4 h. The fluorescence was measured using Tecan Infinite M200 Microplate Reader (Tecan Austria GmbH A-5082, GrÖdig, Austria) with excitation at 530 nm and emission at 590 nm. Each experiment was repeated three times.

To study the growth curve of *SLC13A3* gene knockdown or knockout cells, HepG2- and SNU398-sh*NC* and sh*SLC13A3* or sg*Control* and sg*SLC13A3* cells were seeded into 96 well plate, followed by transfection with empty vector (*EV*) or *SLC13A3* overexpression plasmid, respectively. To determine the role of ATG5, cells were transfected with negative control siRNA or *ATG5* siRNA for 6 h, and then cultured in the complete medium for the indicated time points. To determine the effect of leucine, GSH or NAC on *SLC13A3* knockdown cells, stably *SLC13A3*-knockdown HepG2 and SNU398 cells were treated with 2 mM leucine, 5 mM GSH, or 2 mM NAC for the indicated time points.

To determine the mechanism underlying the cell death, cells were treated with various compounds (NSA, 5 and 10 μM; ZVAF, 0.5 and 1 μM; CQ, 1 μM; BafA1, 100 nM; Fer-1, 1 μM; Lip-1, 1 μM) for 48 h. To determine the cytotoxicity of ACA, cells were treated with various concentrations of ACA (0, 3.125, 6.25, 12.5, 25, 50, 100 and 200 μM) alone or 20 μM ACA together with sorafenib (0, 0.5, 1, 2, 4 μM). To investigate the potential off-target effect of ACA, stably *SLC13A3*-knockdown HepG2 and SNU398 cells were transfected with respective overexpressing plasmids (*EV, PLA2, AP2M1, TRPM2, SLC13A3, or SLC13A5*) for 6 h, followed by ACA treatment at different concentration. To determine the effect of ferroptosis, HepG2 and SNU398 cells with or without *SLC13A3* knockdown were treated with sorafenib (0, 1.25, 2.5, 5, and 10 μM), erastin (0, 1.25, 2.5, 5, and 10 μM), RSL3 (0, 0.025,0.05, 0.1, and 0.5 μM), BSO (0, 1.25,2.5, 5, and 10 mM) or AF (0, 1.25, 2.5, 5, and 10 μM) for 48 h. The combination assay was performed by adding 10 μM sorafenib with 5 mM GSH or 2 mM NAC together. The vehicle control was DMSO (final concentration <0.5%).

### Colony formation assay

Cells were treated with the indicated compound for 24 h, trypsinized, pelleted and resuspended in cell culture medium (2000 cells/mL). Cell suspension was mixed with 0.9% agar solution at 1:1 ratio, and then

https://doi.org/10.1038/s41467-024-51860-2

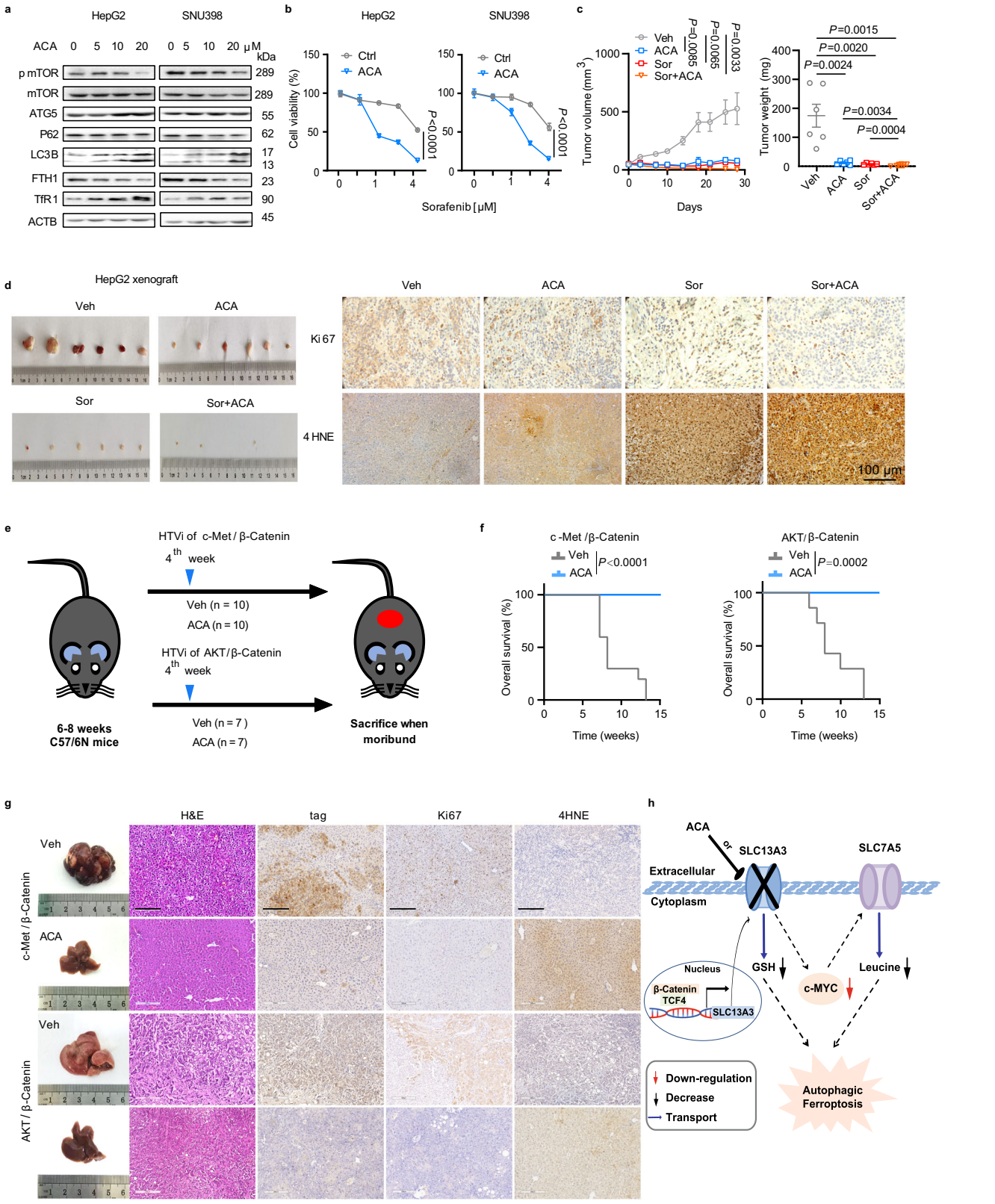


plated into a 24-well plate (0.5 mL/well). Cells were cultured for 2 weeks with the medium changed every two days. By the end of experiment, cell medium was discarded and washed with PBS twice. Cell colonies were stained with 200 μL of crystal violet solution (Solarbio Life Science, Beijing, China), and the photographs of cell colonies were analyzed using Image J software (National Institutes of Health, Bethesda, MD, USA). Each experiment was repeated three times.

### Uptake assay

Cells were seeded into 12-well plates pre-coated with poly-D-lysine (0.1 mg/mL) for 24 h. For leucine uptake, after cells were incubated with pre-warmed uptake buffer for 5 min at 37 °C, uptake was initiated by adding leucine (0, 2 mM) for 20 min at 37 °C. The uptake was terminated by adding cold uptake buffer, and washed with cold PBS three times. Cell lysates (in 200 μL of water) were obtained after three

**Fig. 7 | ACA suppresses the growth of β-catenin-activated HCCs.** **a** Representative western blots of pmTOR, mTOR, ATG5, p62, LC3B, FTH1, and TfR1 in HepG2 and SNU398 cells after treatment with ACA (0, 5, 10, 20 μM) for 48 h ($n = 3$ independent experiments). **b** Cytotoxicity of 20 μM ACA in HepG2 and SNU398 cells co-treated with sorafenib (0, 0.5, 1, 2, 4 μM) for 48 h. The gray curve was the vehicle control DMSO group, the blue curve was ACA group. Data are presented as the mean ± SEM ($n = 3$ independent experiments). Statistical analysis was performed using two-tailed Student's $t$ test. **c** Tumor volumes and weights of HepG2 xenografts after treatment with vehicle (Veh, 5% DMSO + 40% PEG400 + 55% saline, gray), ACA (30 mg/Kg, i.p., once every two days, blue), sorafenib (Sor, 10 mg/Kg, i.p., once every two days, red), or combination of sorafenib and ACA (Sor+ACA, 30 mg/kg ACA + 10 mg/kg Sorafenib, i.p., once every two days, orange). Data are presented as the mean ± SEM ($n = 6$ independent mice per group). Statistical analysis was performed using one-way ANOVA test. **d** Gross images and representative IHC staining images of HepG2 xenografts. Images were representative shown out of 6 independent mice per group. **e** Study design. Mice were subjected to hydrodynamic tail vein injection (HTVi) of c-Met/β-catenin plasmids or AKT/β-catenin plasmids. Starting from 3 weeks post injection, mice were treated with vehicle (Veh, 5% DMSO + 40% PEG400 + 55% saline) or ACA (30 mg/Kg, i.p., once every two days). **f** Survival curves. Mice were euthanized when they developed a high burden of liver tumors (Gray curve, vehicle control group; Blue curve, ACA-treated group). The log-rank test was used to compare overall survival between groups. **g** Representative gross liver images, as well as H&E and IHC staining images. Images were representative shown out at least 7 independent mice per group. Scale bar, 200 μm. **h** Scheme summarizing the effect of SLC13A3 inhibition on intracellular metabolic pathways that ultimately converge on autophagic ferroptosis in β-catenin-activated HCC cells. Source data are provided as a Source Data file.

freeze-thaw cycles (-80 °C to 37 °C). Cell extraction was performed by mixing 180 μL of lysates with 360 μL of methanol, and centrifuged at 13400 x g for 20 min at 4 °C. The supernatant was subjected to UHPLC-MS/MS. Total protein concentrations of cell lysates were measured using the BCA protein assay kit (CoWin Biosciences, Beijing, China). The concentrations in cell lysates were normalized with total protein.

For GSH uptake assay in HEK293 cells, HEK-*EV* and HEK-*SLC13A3* cells were seeded into 12-well plates pre-coated with poly-D-lysine, and then cultured for 24 h to allow adherence. Uptake of gluthathione-(glycine-$^{13}C_2$,$^{15}N$) (0, 10, 50 nM; 0.2, 1, 10, 20, 100, 500 μM; 1, 2, 10 mM) were conducted as mentioned above for 20 min at 37 °C. Uptake was terminated using cold uptake buffer. Cells were lysed, and metabolites were extracted by mixing 180 μL of cell lysates with 360 μL of methanol, and centrifuged at 13,400 × $g$ for 20 min at 4 °C. The supernatant was subjected to UPLC-MS for GSH quantification. The concentrations of metabolites in cell lysates were normalized with cell number.

To determine the effect of GSH on succinic acid uptake, we first generated transient *SLC13A3*-overexpressing HEK293 cells. Transient transfection involved the use of a plasmid construct encoding *SLC13A3* (Origene, Cat#: SC310225) and an empty vector control (pCMV6-Entry), achieved through reverse transfection utilizing Lipofectamine LTX transfection reagent (Thermo Fisher Scientific) following the manufacturer's protocol. The constructs were mixed with Lipofectamine LTX in OptiMEM (Life Technologies), vortexed for 10 seconds, allowed to stand at room temperature for 15 min, and then added to poly-D-lysine–coated 96-well plates (PerkinElmer, Cat# 6005040). Each well received 100 ng DNA and 0.2 μL of Lipofectamine LTX. HEK293 cells were counted and seeded into wells at a density of approximately 40,000 cells/0.1 mL approximately 48 h prior to uptake studies. Prior to uptake studies, the culture medium was removed, and cells were incubated in HBSS for 10–20 min at 37 °C. An assay mixture consisting of $^{14}C$-succinic acid (Moravek, Cat#MC 238, diluted 1:4000) and varying concentrations of GSH (Sigma, Cat#G4251) was prepared and incubated at 37 °C for 15 min. Uptake reactions were terminated by washing cells three times with 300 μL of ice-cold HBSS buffer, followed by incubation in 100 μL of MicroScint fluid (PerkinElmer) on a shaker for 1 h. Radioactivity was measured using a liquid scintillation counter (MicroBeta2® microplate counter, PerkinElmer).

### Metabolomics assay

Cells were cultured in 10 cm dishes for 24 h, and harvested by scrapping and counting cell number to $8 \times 10^6$/sample. Samples were quickly washed twice with cold PBS, and were extracted by directly adding 0.5 mL of 70% methanol (in water). Cell lysate ($n = 6$ independent dishes of each group) was obtained after repeating freeze/thaw (snap-frozen in liquid nitrogen and warm at 37 °C) for three times. After centrifuging at 13,400 × $g$ for 20 min at 4 °C, the supernatant was collected. Untargeted metabolomics was performed in a Thermo Fisher Scientific U3000 UHPLC equipped with Q Exactive™ Q-Orbitrap MS through HESI source (Thermo Fisher Scientific, Waltham, MA, USA). Chromatographic separation was achieved on a Waters BEH C18 column (2.1 × 100 mm, 1.7 μm) (Waters, Milford, MA, USA). The mobile phases were A (100% acetonitrile) and B (0.1% formic acid in water) with the linear gradient: phase A started with 98% at 0-2 min, decreased to 2% until 14 min (2-14 min), maintained at 2% for 3 min (14-17 min), increased to 98% within 17–17.1 min, and then kept at 98% within 17.1–20 min. The flow rate of the mobile phase was 0.3 mL/min. The column temperature was 40 °C. The injection volume was 5 μL. The positive and negative IonSpray Voltage Floating (ISVF) of ionization source conditions were 5 kV and −4.5 kV, respectively. The collision energy was ± 35 eV with ± 80 eV of the declustering potential. The scanning mass range of m/z was 40–1000. A quality control (QC) sample comprising an aliquot of every sample was used to monitor the stability of the instrument. QC sample was conducted between 5 samples throughout the analytical run.

### Metabolomics multivariate analysis

Raw data were analyzed using Compound Discoverer 3.2 software (ThermoFisher Scientific). The metabolites were identified by comparing with standards (including $t_R$, MS, and $MS^2$ information), in-house database, and the METLIN database (http://metlin.scripps.edu/index.php). All data were normalized and analyzed using SIMCA 14.1 software (Umetrics, Sweden). Orthogonal partial least square discriminate analysis (OPLS-DA) was used to visualize the group differences. S-plot analyses were referred to VIP > 1 (variable importance in projection value) for OPLS-DA and $p < 0.05$ from $t$-test. Each point represented a metabolite.

### mRFP-GFP-LC3 transfection and confocal microscopy

Cells were seeded on cover glasses in 24-well plates ($5 \times 10^4$ cells/well) and cultured in the complete medium. Cells were then transfected with 1 μg mRFP-GFP-LC3 plasmid in 3 μL of PEI (1 mg/mL). After 24 h, cells were fixed with 4% paraformaldehyde for 20 min and washed with PBS three times. Cells were mounted onto slice and imaged using Nikon confocal microscopy (Nikon ECLIPSE 80i, Tokyo, Japan).

### Immunofluorescence and confocal microscopy

HepG2/SNU398-sh*NC* and -sh*SLC13A3* cells were seeded in 12-well plates ($6 \times 10^5$ /well) with round glass slide placed inside for 24 h. Cells were fixed with 4% paraformaldehyde for 20 min, washed with PBS three times, permeabilized with 0.1% Triton-X-100 for 10 min, and then washed with PBS three times. Cells were blocked with 3% BSA for 2 h, and then were incubated with LC3B antibody (1:1600, 3868S, Cell Signaling Technology, San Antonio, TX, USA) at 4 °C overnight. After being washed with 0.05% PBST for 3 times, cells were incubated with secondary antibody (1:500, BA1105, Boster, Pleasanton, CA, USA) for 1 h at room temperature. After being washed with PBST for 3 times, cells were stained with 0.1 μg/ml DAPI (Sigma-Aldrich, St. Louis, MO) for 5 min. After PBST wash three times, cells were mounted onto slice

and imaged using Nikon confocal microscopy (Nikon ECLIPSE 80i, Tokyo, Japan).

### Luciferase assay

HEK293T cells were plated in a 96-well plate ($5 \times 10^4$ /well) overnight, and transfected with plasmids (60 ng pGL4-*CTNNB1*, 30 ng pCMV-renilla, and 60 ng pCMV-*hSLC13A3* promoter constructs). After 6 h transfection, cells were changed with fresh medium containing 5% FBS. After 24 h, cells were collected to determine firefly and renilla luciferase activities using the Dual-Glo luciferase assay system kit (Promega Inc, Madison, WI, USA) in a Tecan Infinite M200 Microplate Reader (Tecan Austria GmbH, A-5082 Grödig, Austria). The luciferase activity was normalized with that of renilla.

### Western blot

Total proteins were extracted from cells or tissues using RIPA lysis buffer (Solarbio, Life Science, Beijing, China). For the isolation of membrane proteins, cells were scraped, washed with PBS once, and centrifuged at 300 g for 5 min. The cell pellet was mixed with 100 µL of 10% IGEPAL® CA-630 (Sigma-Aldrich, St. Louis, MO) and incubated on ice for 10 min. After centrifugation at 16,000 g for 15 min, the supernatant was discarded. The precipitated pellet was resuspended in 100 µL of lysis buffer (10 mM Hepes, pH 8.0; 1.5 mM $MgCl_2$; 10 mM KCl; 1 mM DTT; 50 × protease inhibitor) and then incubated on ice for 30 min. After centrifugation at 16,000 g for 15 min, the supernatant containing membrane proteins was collected. The concentrations of proteins were determined using a BCA protein assay kit (CWBIO Bio Inc., Haidian, Beijing, China). Total proteins were denatured by the addition of loading buffer (Sigma-Aldrich, St. Louis, MO) and boiling at 100 °C for 5 min, whereas membrane proteins were treated with loading buffer without heat treatment. Proteins were separated by electrophoresis on 8-12% SDS PAGE, and transferred onto PVDF membranes (Merck Millipore, Darmstadt, Germany). Membranes were blocked with 5% dried skimmed milk for 2 h, followed by incubation with primary antibodies overnight at 4 °C and secondary antibodies for 90 min at room temperature (see Supplementary Data 6 for antibody information). The protein bands were visualized using the Amersham Imager 600 (GE Healthcare, Marlborough, MA, USA) after reacting with ECL Western blotting detection reagents (Advansta Inc., San Jose, CA, USA). The relative protein levels were quantified using Image J software. The statistical analysis data of all western blots are summarized in Supplementary Fig. 18-22.

### Real-time qPCR

Total RNA was extracted using TRIzol (Takara Biomedical Technology Co., Ltd.,Beijing, China) according to the manufacturer's protocol. RNA was transcribed into cDNA using HiScript Q-RT SuperMix for qPCR (VazymeBiotech, Nanjing, Jiangsu, China). Quantitative real-time PCR was performed on an ABI Quant Studio 6 Flex Real-Time PCR system (Applied Biosystems, Foster City, CA, USA) using Ultra SYBR Mixture (CWBIO Bio Inc., Beijing, China). The comparative threshold cycle (Ct) method was used to determine the fold change ($2^{-\Delta\Delta Ct}$) in mRNA levels of various genes. The mRNA levels were normalized to the reference gene *m36b4* or *h36B4*. Primer sequences were listed in Supplementary Data 7.

### Flow cytometric analysis

For apoptosis assay, $1 \times 10^5$ cells were harvested, washed with cold PBS twice, resuspended in 200 µL of 1xbinding buffer, stained with 5 µL of Annexin V-FITC and 5 µL of PI (Annexin V-FITC/PI Apoptosis Detection Kit, Suzhou Meilun Biotechnology Co., Ltd., Jiangsu, China) for 15 min at 4 °C. The percentage of cell apoptosis was determined using flow cytometry (BD Biosciences AccuriC6, Becton, Dickinson and Company, Franklin Lakes, NJ, USA).

For C11-BODIPY staining assay, $1 \times 10^5$ cells were washed with PBS three times, incubated with 200 µL of 2% FBS-PBS (2 µL of FBS in 198 µL of PBS) containing 5 µM C11-BODIPY (Thermo Fisher Scientific, Gaithersburg, MD, USA) for 30 min at 37 °C. Cells were washed with PBS and then resuspended in 2% FBS-PBS for flow cytometric analysis.

### Caspase 3/7 activity assay

Cells were seeded into white 96-well plates ($5 \times 10^4$) and cultured overnight for adherence. Caspase-3/7 activity was determined using the Caspase-Glo 3/7 assay system kit (Promega, Madison, WI).

### Chromatin immunoprecipitation (ChIP) assay

HepG2 cells were seeded in 10 cm dishes and cultured for 24 h. ChIP assays were performed following the manufacturer's protocol using a commercial ChIP kit (ab500, Abcam, Cambridge, MA). β-Catenin antibody (8480S, Cell Signaling Technology, San Antonio, TX, USA), TCF4 antibody (2569S, Cell Signaling Technology, San Antonio, TX, USA) were used to pull down the associated DNA which was sheared to 200-700 bp fragments. IgG was used as negative control in each experiment. The immunoprecipitated DNA was isolated, purified, and used as a template for PCR. ChIP-PCR and ChIP-qPCR were amplified using primers specific to the *SLC13A3* promoter (see Supplementary Table 4 for primer sequences). The gel electrophoresis of PCR products was performed on 2% agarose gel, which was stained with GelRed® Nucleic Acid Stain 10000X Water (SCT123, Thermo Fisher Scientific, Gaithersburg, MD, USA) and imaged using BioDoc-It 220 imaging system (Ultra-Violet Products Ltd., CA, USA).

### Methylated DNA immunoprecipitation (MeDIP) assay

HepG2-sh*NC* and -sh*SLC13A3* cells were seeded into 10 cm dishes and then cultured for 24 h. MeDIP assays were performed using a commercial methylated DNA immunoprecipitation (MeDIP) ChIP kit (ab117135, Abcam, Cambridge, MA). DNA was sheared by sonication and incubated initially with anti-5-Methylcytosine antibody (in the kit) or alternatively, with IgG as negative control. The immunoprecipitated DNA was isolated and amplified by PCR using primers targeting methylated islands across the *c-MYC* promoter (see Supplementary Table 4 for primer sequences). The PCR products were measured using real-time PCR and agarose gel electrophoresis, respectively.

### Methylation-specific PCR (MSP)

Genomic DNA from stably *SLC13A3*-knockdown HepG2 and SNU398 cells as well as stably *SLC13A3*-overexpressing HEK293 cells (HEK293-*EV* and HEK293-*SLC13A3*) were extracted using a TIANamp genomic DNA kit (Tiangen Biotech, Beijing, China) according to the manufacturer's instructions. One microgram of genomic DNA per sample was applied using the EZ DNA methylation kit (Zymo Research Corp, Irvine, US) according to the manufacturer's instructions. Methylated primers were designed using Website (http://www.urogene.org/cgi-bin/methprimer/methprimer.cgi) and synthesized by GENEWIZ (Supplementary Table 5). Each reaction was performed in a total reaction volume of 20 µL, containing 1 µL of MSP primer mix (10 µM), 1 µL of bisulfite-treated DNA, 0.4 µL of dNTPs (10 mM), and 0.5 U AmpliTaq Gold DNA polymerase. The MSP thermal cycling program was as follows: 10 min at 95 °C; 95 °C for 60 s, 65 °C for 60 s, and 72 °C for 60 s, for a total of 50 cycles; with a final elongation step of 7 min at 72 °C.

### Electrophoretic mobility shift assay (EMSA)

Cell nuclear extracts of HepG2 cells were subjected to EMSA assay by using the nuclear extraction protocol. Protein concentrations were determined using a BCA protein assay kit (CWBIO Bio Inc., Beijing, China). Both 5′- and 3′- biotin-labeled wild-type *SLC13A3* probe #1 (5′-ctagtacctgctttgttggggtatggt-3′) or mutated probe #1 (5′-ctagtacctgtatttgtggggtatggt-3′), wild-type *SLC13A3* probe #2 (5′-tccgtgctgttctcgtgatagcgagtgagttctcacgagatctgatggt-3′) or mutated

probe #2 (5′-tccgtgctgttctcgtgacagagcttgagttctcacgagatctgatggt-3′) were obtained from GENEWIZ (Tianjin, China). The reaction mixtures (1 μg HepG2 nuclear protein, 1 pmol probes annealed on 95 °C for 5 min in a heat block, 1 μg poly d(I-C), 2 μL of 5X Binding Buffer, 1.0 μL of TF probe, 2.0 μL of cold TF probe for competitive group, 1.5 μL of anti-TCF4 antibody for supershift band) were incubated according to manufacturer's protocol and then loaded on a 6% native polyacrylamide gel in 0.5% TBE buffer and blotted onto Biodyne™ B Nylon Membrane (0.45 μm, Thermo Fisher Scientific, Gaithersburg, MD, USA). After 10 min of UV cross-linking, the interaction between the biotin-labeled *SLC13A3* probes and the TCF4 protein was detected using LightShift™ chemiluminescent EMSA kit (20148, Thermo Fisher Scientific, Gaithersburg, MD, USA).

### Lipid peroxidation assay (MDA level)

The malondialdehyde (MDA) concentrations in cell lysates (prepared by repeated freeze-thaw in liquid nitrogen) were measured using a commercial lipid peroxidation (MDA) assay kit (Jiancheng Biological Technology, Nanjing, Jiangsu, China) according to the manufacturer' instructions. MDA concentrations were then normalized with protein concentrations which were measured using a BCA protein assay kit (CWBIO Bio Inc., Beijing, China).

### Lipid peroxidation assay (C11-BODIPY detection)

Cells were seeded into white 24-well plates ($1 \times 10^5$) and cultured overnight for adherence. Cells were treated with autophagy inhibitors (CQ, 1 μM; BafA1, 100 nM) for 24 h or transfected with *ATG5* siRNA for 24 h. Cells were washed with PBS three times, incubated with 500 μL of 1 μM C11-BODIPY in 2% FBS-PBS for 15 min at 37 °C. Cells were then washed with PBS and measured by Tecan Infinite M200 Microplate Reader with excitation at 510 nm and emission at 590 nm. Each experiment was repeated three times.

### Reactive Oxygen Species (ROS) measurement

Stably *SLC13A3*-knockdown HepG2 and SNU398 cells were established as mentioned above. Cells were seeded into 96-well plates ($1 \times 10^4$cells/well) and cultured overnight. After cells were washed with DMEM medium for three times, they were cultured in DMEM with DCFH-DA (10 μM in DMEM medium) at 37 °C for 30 min. The ROS level was assessed using a reactive oxygen species assay kit (Jiancheng Biological Technology, Nanjing, Jiangsu, China) following the manufacturer's instructions by Tecan Infinite M200 Microplate Reader with excitation at 488 nm and emission at 525 nm. Fluorescent images were taken by Nikon confocal microscopy (Nikon ECLIPSE 80i, Tokyo, Japan).

### Glutathione (GSH) measurement

Stably *SLC13A3*-knockdown HepG2 and SNU398 cells were established as mentioned above. Cells were seeded into 96-well plates ($1 \times 10^4$cells/well) and cultured overnight for adherence (cultured in DMEM + 10% dialyzed FBS). After cells were washed with cold PBS three times, they were cultured in DMEM with 10% FBS complete medium. GSH was quantified at 0, 10, 20, 40 and 60 min. The level of GSH was assessed using a reduced glutathione (GSH) assay kit (Jiancheng Biological Technology, Nanjing, Jiangsu, China) following the manufacturer's instructions by measuring the OD value at 420 nm.

### Animals

BALB/C male nude mice and C57BL/6 N male mice (6-8 weeks old) from Beijing Vital River Laboratory Animal Technology Co., Ltd (Beijing, China) were housed in a certified animal facility (temperature: 23 ± 2 °C, humidity: 55 ± 10%, 12 h dark/light cycles) at CAMS, with ad libitum access to water and standard diet (233 g/Kg protein, 59 g/Kg fat). The diet (Catalogue NO.1022) was obtained from Beijing HFK BIOSCIENCE CO., LTD (Beijing, China). Because we did not observe obvious differences of SLC13A3 expression between male and female human HCC tissues, we chose to use male mice for the present study. All protocols were approved by CAMS Animal Ethics Committee (No.IRM-DWLL-2021177). Animal handling was in accordance with ARRIVE Guidelines 2.0 and CAMS Guide for Care and Use of Laboratory Animals.

For HepG2 cell xenograft study, HepG2 cells ($1 \times 10^7$ cells per mouse) were subcutaneously injected to the left back of male BALB/C nude mice (6-8 weeks old). Tumor volume was measured using vernier caliper. When tumor volume reached about 50 $mm^3$ (volume=length x $width^2/2$), mice were administered shRNA lentivirus (sh*NC*, negative control shRNA lentivirus; sh*SLC13A3*, *SLC13A3* specific shRNA lentivirus, 4 mice per group) via intratumor injection three times in two days. Tumor volumes and body weights were measured every three days.

For the ferroptosis inhibitor study, HepG2 cells ($1 \times 10^7$ cells per mouse) were subcutaneously injected to the left back of male BALB/C nude mice (6-8 weeks old, n = 6, 4 groups). When tumor volume reached about 50 $mm^3$ (volume=length x $width^2/2$) about 2 weeks post-transplantation, mice were subjected to intratumor injection of shRNA lentiviruses (sh*NC*, netagtive control shRNA; sh*SLC13A3*, *SLC13A3* shRNA) as mentioned above. After the injection, mice were intraperitoneally injected with 10 mg/kg Liproxstatin-1 (dissolved in saline containing 1% DMSO) or vehicle once every two days for 4 weeks. Body weights and tumor volumes were measured every three days.

For toxicity study of ACA, 6–8-week-old male BALB/C nude mice and male C57BL/6 N mice ($n = 4 \sim 5$ mice per group) were administered either vehicle (saline with 5% DMSO and 40% PEG400) or 60 mg/kg ACA (i.p., once every two days) for 2 weeks. Body weights were measured every three days.

For ACA treatment in HepG2 cell xenografts, 6-8 weeks old male BALB/C nude mice were divided into 4 groups. When tumor volume reached about 50 $mm^3$, mice were treated with vehicle (saline with 5% DMSO and 40% PEG400), 30 mg/kg ACA, 10 mg/kg sorafenib, or 30 mg/kg ACA and 10 mg/kg sorefenib (n = 6 mice per group). Body weights and tumor volumes were measured every three days.

For ACA treatment in β-catenin-driven mouse liver tumor models, 6-8 weeks male C57BL/6 N mice were transfected with c-Met/β-catenin plasmids (2 mL of saline containing 20 μg pT3-EF1αH c-Met plasmid, 20 μg pT3-EF1αH N90-beta-catenin plasmid, and 1.6 μg pCMV/sleeping beauty transposase plasmid) or AKT/β-catenin plasmids (2 mL of saline containing 20 μg pT3-EF1αH myr-AKT-HA plasmid, 20 μg pT3-EF1αH N90-beta-catenin plasmid, and 1.6 μg pCMV/sleeping beauty transposase plasmid) via hydrodynamic tail vein injection within 5 to 7 seconds. Starting from the $4^{th}$ week post-injection, mice were intraperitoneally administered 30 mg/kg ACA or vehicle (saline with 5% DMSO and 40% PEG400) once every two days ($n = 7–10$ mice per group).

For shRNA lentivirus treatment, 6-8 weeks male C57BL/6N mice were co-administered c-Met/β-catenin plasmids or AKT/β-catenin plasmids together with sh*NC* or sh*Slc13a3* lentivirus via hydrodynamic tail vein injection within 5 to 7 seconds ($n = 6–10$ mice per group). Mice were sacrificed when they were in critical condition.

For leucine treatment, leucine deficient diet was purchased from Jiangsu Xietong Pharmaceutical Bio-engineering Co., Ltd. (Catalogue No.#20231028, Jiangsu, China). Leucine control diet was obtained from the same company which contained 180.2 g/Kg total L-amino acids. Leucine supplementation was achieved by adding 1.5% (w/v) leucine powder (Solarbio Life Science, Beijing, China) in drinking water. Male C57BL/6 N mice (6-8 weeks) adapted to respective diets two days prior to transfection with c-Met/β-catenin plasmids or AKT/β-catenin plasmids via hydrodynamic tail vein injection. Mice were sacrificed when they were in critical condition (n = 6 mice per group).

For *Slc13a3* knockout treatments, 6-8 weeks old male C57BL/6 N mice were intravenously injected with adeno-associated virus (AAV-8, sg*Control* or sg*Slc13a3*, n = 6 mice per group). Two weeks post-virus

infection, mice were transfected with c-Met/β-catenin plasmids or AKT/β-catenin plasmids via hydrodynamic tail vein injection. Mice were sacrificed when they were in critical condition.

### H&E and immunohistochemistry (IHC)

Tissue samples were fixed in 10% buffered formalin and embedded in paraffin, and cut into 5 μm sections. For H&E staining, sections were deparaffinized, rehydrated, and stained with haematoxylin and eosin (Baso, Zhuhai, Guangdong, China). For IHC staining, sections were deparaffinized, rehydrated, and then antigens were recovered in 10 mM citrate buffer (pH 6.0) for 10 min in a microwave oven. $H_2O_2$ (3%) was used to block endogenous peroxidase, followed by PBS wash. After sections were blocked in 5% goat serum (Spark Jade, Qingdao, Shandong, China) at room temperature for 10 min, they were incubated with primary antibodies for Ki67 (CST, Shanghai, China, 1:800), SLC13A3 (Atlas Antibodies, Stockholm, Sweden, 1:200), cleaved caspase 3 (Cell Signaling Technology, San Antonio, TX, USA, 1:200), MYC-tag (Cell Signaling Technology, San Antonio, TX, USA, 1:200), HA-tag (Cell Signaling Technology, San Antonio, TX, USA, 1:200), or 4HNE (R&D Systems, Minneapolis, MN, USA) overnight at 4 °C. The information of antibodies used for IHC was shown in Supplementary Table 6. The sections were then washed with PBS, incubated with peroxidase-labeled secondary antibodies (Absin, Shanghai, China, 1:1000) at 37 °C for 2 h, and washed with PBS. Sections were stained with 3,3′-diaminobenzidine (Spark Jade, Qingdao, Shandong, China) and then counter-stained with hematoxylin (BaSO, Zhuhai, Guangdong, China). The quantification was performed using Image Pro Plus software version 6.0 and the statistical analyses were shown in Supplementary Fig. 19 and Supplementary Fig. 21.

### Human subjects

Human hepatocellular carcinoma tissue microarrays were obtained from Outdo Biotech Inc. (Shanghai, China), which contained 82 HCC cases with corresponding adjacent normal tissues. The sex and/or gender, number and age of participants in human project were provided in Source Data files. HCC patients donated organs voluntarily and informed consent was obtained from patients before tissue collection. The company has approved human hepatocellular carcinoma tissue microarrays (No. YB M-05-02). IHC staining was performed as described above. The tissue microarrays were digitized using Aperio scanners (Aperio XT, LEICA, Germany). The results of IHC staining were assessed blindly by Dr. Wei Zhang, a certified pathologist at Tianjin Medical University (Tianjin, China), according to the staining area and intensity. IHC analyses were scored as follows: grade 0, score = 1–2; grade 1, weak expression, score = 3–4; grade 2, moderate expression, score = 5–6; and grade 3, intense expression, score = 7–8.

### Blood biochemistry analyses

Serum ALT (alanine aminotransferase), AST (aspartate aminotransferase), ALP (alkaline phosphatase), and BUN (blood urea nitrogen) were determined using commercial kits (Jiancheng Biological Technology, Nanjing, Jiangsu, China).

### Statistics and reproducibility

All data were expressed as the mean ± SEM (standard error of mean). Statistical comparisons were made using one-way analysis of variance (ANOVA) for more than two groups or Student's *t* test for comparison between two groups. Statistical significance was considered with *P* value of 0.05 or less. *P* values were marked in the corresponding figures. Survival comparisons were performed using a Log Rank test. Pearson correlation and linear regression were used to determine the correlation in clinical samples. All statistics were performed using GraphPad Prism 8, version 8.0 (GraphPad Software Inc., La Jolla, CA). For normalization, data points of one experiment were either normalized to the untreated control or divided by the global mean of the individual experiment. We defined one n as one independent biological experiment. The statistics methods were provided in Source data files in individual Excel sheet.

### Reporting summary

Further information on research design is available in the Nature Portfolio Reporting Summary linked to this article.

## Data availability

The public data from TCGA dataset are available at https://portal.gdc.cancer.gov/ and www.cbioportal.org/. The data supporting the findings of this study are available within the article and its Supplementary Information Files. Source data are provided with this paper.

## References


1. Faivre, S., Rimassa, L. & Finn, R. S. Molecular therapies for HCC: Looking outside the box. *J. Hepatol.* **72**, 342–352 (2020).
2. Xu, C. et al. Beta-catenin signaling in hepatocellular carcinoma. *J. Clin. Invest* **132**, e154515 (2022).
3. Yamashita, T., Budhu, A., Forgues, M. & Wang, X. W. Activation of hepatic stem cell marker EpCAM by Wnt-beta-catenin signaling in hepatocellular carcinoma. *Cancer Res* **67**, 10831–10839 (2007).
4. Wei, W., Chua, M. S., Grepper, S. & So, S. Small molecule antagonists of Tcf4/beta-catenin complex inhibit the growth of HCC cells in vitro and in vivo. *Int J. Cancer* **126**, 2426–2436 (2010).
5. Lin, L., Yee, S. W., Kim, R. B. & Giacomini, K. M. SLC transporters as therapeutic targets: emerging opportunities. *Nat. Rev. Drug Discov.* **14**, 543–560 (2015).
6. Nyquist, M. D., Prasad, B. & Mostaghel, E. A. Harnessing solute carrier transporters for precision oncology. *Molecules* **22**, 539 (2017).
7. Pajor, A. M. Sodium-coupled dicarboxylate and citrate transporters from the SLC13 family. *Pflug. Arch.* **466**, 119–130 (2014).
8. Bidkhori, G. et al. Metabolic network-based stratification of hepatocellular carcinoma reveals three distinct tumor subtypes. *Proc. Natl Acad. Sci. USA* **115**, E11874–E11883 (2018).
9. Charawi, S. et al. LKB1 signaling is activated in CTNNB1-mutated HCC and positively regulates beta-catenin-dependent CTNNB1-mutated HCC. *J. Pathol.* **247**, 435–443 (2019).
10. Chen, L. et al. OCT1 is a high-capacity thiamine transporter that regulates hepatic steatosis and is a target of metformin. *Proc. Natl Acad. Sci. USA* **111**, 9983–9988 (2014).
11. Schorbach, L., Krick, W., Burckhardt, G. & Burckhardt, B. C. Glutathione is a low-affinity substrate of the human sodium-dependent dicarboxylate transporter. *Nephron Physiol.* **124**, 1–5 (2013).
12. Yue, M., Jiang, J., Gao, P., Liu, H. & Qing, G. Oncogenic MYC activates a feedforward regulatory loop promoting essential amino acid metabolism and tumorigenesis. *Cell Rep.* **21**, 3819–3832 (2017).
13. Prasad, P. D. et al. Human LAT1, a subunit of system L amino acid transporter: molecular cloning and transport function. *Biochem. Biophys. Res. Commun.* **255**, 283–288 (1999).
14. Broer, S. The SLC38 family of sodium-amino acid co-transporters. *Pflug. Arch.* **466**, 155–172 (2014).
15. Fuchs, B. C. & Bode, B. P. Amino acid transporters ASCT2 and LAT1 in cancer: partners in crime? *Semin Cancer Biol.* **15**, 254–266 (2005).
16. Kim, J., Lee, J. H. & Iyer, V. R. Global identification of Myc target genes reveals its direct role in mitochondrial biogenesis and its E-box usage in vivo. *PLoS ONE* **3**, e1798 (2008).
17. Parsanathan, R. & Jain, S. K. Glutathione deficiency induces epigenetic alterations of vitamin D metabolism genes in the livers of high-fat diet-fed obese mice. *Sci. Rep.* **9**, 14784 (2019).
18. Gougelet, A. et al. T-cell factor 4 and beta-catenin chromatin occupancies pattern zonal liver metabolism in mice. *Hepatology* **59**, 2344–2357 (2014).

19. Tang, D., Chen, X., Kang, R. & Kroemer, G. Ferroptosis: molecular mechanisms and health implications. *Cell Res.* **31**, 107–125 (2021).
20. Feng, H. et al. Transferrin receptor is a specific ferroptosis marker. *Cell Rep.* **30**, 3411–3423.e3417 (2020).
21. Ingold, I. et al. Selenium utilization by GPX4 is required to prevent hydroperoxide-induced ferroptosis. *Cell* **172**, 409–422.e421 (2018).
22. Louandre, C. et al. Iron-dependent cell death of hepatocellular carcinoma cells exposed to sorafenib. *Int J. Cancer* **133**, 1732–1742 (2013).
23. Gao, M. et al. Ferroptosis is an autophagic cell death process. *Cell Res* **26**, 1021–1032 (2016).
24. Adebayo Michael, A. O. et al. Inhibiting glutamine-dependent mTORC1 activation ameliorates liver cancers driven by beta-catenin mutations. *Cell Metab.* **29**, 1135–1150.e1136 (2019).
25. Chen, J. et al. SAR1B senses leucine levels to regulate mTORC1 signalling. *Nature* **596**, 281–284 (2021).
26. Zhu, Y. et al. An Injectable silk-based hydrogel as a novel biomineralization seedbed for critical-sized bone defect regeneration. *Bioact. Mater.* **35**, 274–290 (2024).
27. Bunse, L. et al. Suppression of antitumor T cell immunity by the oncometabolite (R)-2-hydroxyglutarate. *Nat. Med* **24**, 1192–1203 (2018).
28. Pajor, A. M. & Randolph, K. M. Inhibition of the Na+/dicarboxylate cotransporter by anthranilic acid derivatives. *Mol. Pharm.* **72**, 1330–1336 (2007).
29. Huard, K. et al. Optimization of a dicarboxylic series for in vivo inhibition of citrate transport by the solute carrier 13 (SLC13) family. *J. Med Chem.* **59**, 1165–1175 (2016).
30. Yuan, S. et al. Viruses harness YxxO motif to interact with host AP2M1 for replication: a vulnerable broad-spectrum antiviral target. *Sci. Adv.* **6**, eaba7910 (2020).
31. Lue, H. W. et al. Metabolic reprogramming ensures cancer cell survival despite oncogenic signaling blockade. *Genes Dev.* **31**, 2067–2084 (2017).
32. Ganapathy, A. S. et al. AP2M1 mediates autophagy-induced CLDN2 (claudin 2) degradation through endocytosis and interaction with LC3 and reduces intestinal epithelial tight junction permeability. *Autophagy* **18**, 2086–2103 (2022).
33. Zhu, A. X. et al. Effect of everolimus on survival in advanced hepatocellular carcinoma after failure of sorafenib: the EVOLVE-1 randomized clinical trial. *JAMA* **312**, 57–67 (2014).
34. Martinez-Reyes, I. & Chandel, N. S. Mitochondrial TCA cycle metabolites control physiology and disease. *Nat. Commun.* **11**, 102 (2020).
35. Kumar, A. et al. NaCT/SLC13A5 facilitates citrate import and metabolism under nutrient-limited conditions. *Cell Rep.* **36**, 109701 (2021).
36. Li, Z. et al. Silencing of solute carrier family 13 member 5 disrupts energy homeostasis and inhibits proliferation of human hepatocarcinoma cells. *J. Biol. Chem.* **292**, 13890–13901 (2017).
37. Nezami Ranjbar, M. R. et al. GC-MS based plasma metabolomics for identification of candidate biomarkers for hepatocellular carcinoma in Egyptian cohort. *PLoS ONE* **10**, e0127299 (2015).
38. Morine, Y. et al. Essential amino acids as diagnostic biomarkers of hepatocellular carcinoma based on metabolic analysis. *Oncotarget* **13**, 1286–1298 (2022).
39. Buchard, B. et al. Two metabolomics phenotypes of human hepatocellular carcinoma in non-alcoholic fatty liver disease according to fibrosis severity. *Metabolites* **11**, 54 (2021).
40. Shree Harini, K. & Ezhilarasan, D. Wnt/beta-catenin signaling and its modulators in nonalcoholic fatty liver diseases. *Hepatobiliary Pancreat. Dis. Int* **22**, 333–345 (2023).
41. Nishio, Y. et al. L-isoleucine and L-leucine: tumor promoters of bladder cancer in rats. *Science* **231**, 843–845 (1986).
42. Xie, X. L. et al. Long-term treatment with L-isoleucine or L-leucine in AIN-93G diet has promoting effects on rat bladder carcinogenesis. *Food Chem. Toxicol.* **50**, 3934–3940 (2012).
43. Liu, K. A., Lashinger, L. M., Rasmussen, A. J. & Hursting, S. D. Leucine supplementation differentially enhances pancreatic cancer growth in lean and overweight mice. *Cancer Metab.* **2**, 6 (2014).
44. Kawaguchi, T. et al. Branched-chain amino acids prevent hepatocarcinogenesis and prolong survival of patients with cirrhosis. *Clin. Gastroenterol. Hepatol.* **12**, 1012–1018.e1011 (2014).
45. Ichikawa, K. et al. Oral supplementation of branched-chain amino acids reduces early recurrence after hepatic resection in patients with hepatocellular carcinoma: a prospective study. *Surg. Today* **43**, 720–726 (2013).
46. Ericksen, R. E. et al. Loss of BCAA catabolism during carcinogenesis enhances mTORC1 activity and promotes tumor development and progression. *Cell Metab.* **29**, 1151–1165.e1156 (2019).
47. Kennedy, L., Sandhu, J. K., Harper, M. E. & Cuperlovic-Culf, M. Role of glutathione in cancer: from mechanisms to therapies. *Biomolecules* **10**, 1429 (2020).
48. Ballatori, N., Krance, S. M., Marchan, R. & Hammond, C. L. Plasma membrane glutathione transporters and their roles in cell physiology and pathophysiology. *Mol. Asp. Med.* **30**, 13–28 (2009).
49. Komarov, D. A. et al. In vivo extracellular ph mapping of tumors using electron paramagnetic resonance. *Anal. Chem.* **90**, 13938–13945 (2018).
50. Ikebuchi, M. et al. Effect of medium pH on glutathione redox cycle in cultured human umbilical vein endothelial cells. *Metabolism* **42**, 1121–1126 (1993).
51. Duval, A. P., Troquier, L., de Souza Silva, O., Demartines, N. & Dormond, O. Diclofenac potentiates sorafenib-based treatments of hepatocellular carcinoma by enhancing oxidative stress. *Cancers (Basel)* **11**, 1453 (2019).
52. Wan, J. et al. Synergistic antitumour activity of sorafenib in combination with tetrandrine is mediated by reactive oxygen species (ROS)/Akt signaling. *Br. J. Cancer* **109**, 342–350 (2013).
53. Yao, X., Zhao, C. R., Yin, H., Wang, K. & Gao, J. J. Synergistic antitumor activity of sorafenib and artesunate in hepatocellular carcinoma cells. *Acta Pharm. Sin.* **41**, 1609–1620 (2020).
54. Wang, H. et al. Targeting Wnt/beta-catenin signaling exacerbates ferroptosis and increases the efficacy of melanoma immunotherapy via the regulation of MITF. *Cells* **11**, 3580 (2022).
55. Lin, H. H. et al. Inhibition of the Wnt/beta-catenin signaling pathway improves the anti-tumor effects of sorafenib against hepatocellular carcinoma. *Cancer Lett.* **381**, 58–66 (2016).


## Acknowledgements

This work was supported by the National Natural Science Foundation of China (NSFC) grant 82274031 to Y.Z., the National Institutes of Health (NIH) grant R01CA221916 to A.S., R01CA250227 to X.C., the Key R&D Projects in the Tianjin Science and Technology Pillar Program 19YFZCSY00420 to C.Z., and the Major Program from National Natural Science Foundation of China (NSFC) grant 82192914 to L.H. The authors thank the current and previous members (Hang Yu and Huiying Li) in Dr. Youcai Zhang and Dr. Dexin Kong's lab for their assistance with the study. The authors also thank Dr. Wei Du and Dr. Wei Zhang for their assistance with IHC and EMSA studies.

## Author contributions

W.Z., X.W., X.C., and Y.Z. conceived and designed the studies. W.Z., X.W., L.H., C.Z., C.W., T.X., M.Z., G.L., J.L., G.H., J.Y., and D.K. generated data, key reagents, and samples. W.Z., X.W., L.H., C.W., and Y.Z. analyzed and interpreted the data. S.W.Y., A.S., X.C., and Y.Z. revised the manuscript. Y.Z. wrote the manuscript. All authors have read and approved the manuscript.

## Competing interests
The authors declare no competing interests.

## Additional information
**Supplementary information** The online version contains supplementary material available at https://doi.org/10.1038/s41467-024-51860-2.

**Correspondence** and requests for materials should be addressed to Xin Chen or Youcai Zhang.

**Peer review information** *Nature Communications* thanks Giovanni Perini, Xin Wang and the other anonymous reviewer(s) for their contribution to the peer review of this work. A peer review file is available.